# The impact of solar and atmospheric parameter uncertainties on the measurement of $\theta_{13}$ and $\delta$

A. Donini <sup>a</sup> D. Meloni <sup>b</sup> S. Rigolin <sup>a</sup>

<sup>a</sup>I.F.T. and Dep. Física Teórica, Univ. Autonoma Madrid., E-28049, Madrid, Spain

<sup>b</sup>INFN, Sezione di Roma e Dip. di Fisica, Univ. di Roma "La Sapienza", P.le A. Moro 2, I-00185 Roma, Italy

PACS: 14.60.Pq, 14.60.Lm

#### Abstract

We present in this paper the analysis of the measurement of the unknown PMNS parameters  $\theta_{13}$  and  $\delta$  at future LBL facilities fully including, for the first time, the errors on the known atmospheric and solar oscillation parameters. We show that, due to the presence of degeneracies, present uncertainties on  $\theta_{23}$  and  $\Delta m_{23}^2$ , worsen significantly the precision on  $(\theta_{13}, \delta)$  at future LBL experiments. On the other hand, the impact on this measurement of the uncertainties on the solar parameters,  $\theta_{12}$ and  $\Delta m_{12}^2$  is already negligible. Only if a precision on the atmospheric parameters at least similar to what expected at T2K-I is reached, then the sensitivities to  $\theta_{13}$  and  $\delta$  that have been presented in the literature for many facilities (where  $\theta_{23}$ and  $\Delta m_{23}^2$  are generally considered as fixed external inputs) can indeed be almost recovered. Our analysis has been performed using three reference setups: the SPL Super-Beam and the standard low- $\gamma$   $\beta$ -Beam, both aiming toward a Mton Water Cerenkov detector located at L = 130 km; the 50 GeV Neutrino Factory with a 40 kton Magnetized Iron Detector to look for the "golden channel"  $\nu_e \rightarrow \nu_\mu$  with baseline L = 3000 km and a 4 kton Emulsion Cloud Chamber to look for the "silver channel"  $\nu_e \to \nu_\tau$  with baseline L = 732 km.

#### 1 Introduction

The results of atmospheric, solar, accelerator and reactor [1] neutrino experiments show that flavour mixing occurs not only in the hadronic sector, as it has been known for long, but in the leptonic sector as well. The experimental results point to two very distinct mass differences  $^1$ ,  $\Delta m_{sol}^2 \approx 8.2 \times 10^{-5} \text{ eV}^2$  and  $|\Delta m_{atm}^2| \approx 2.5 \times 10^{-3} \text{ eV}^2$ . Only two out of the four parameters of the three-family leptonic mixing matrix  $U_{PMNS}$  [4] are known:  $\theta_{12} \approx 32^{\circ}$  and  $\theta_{23} \approx 45^{\circ}$ . The other two parameters,  $\theta_{13}$  and  $\delta$ , are still unknown: for the mixing angle  $\theta_{13}$  direct searches at reactors [5] and three-family global analysis of the experimental data [6,7] give the upper bound  $\theta_{13} \leq 11.5^{\circ}$ , whereas for the leptonic CP-violating phase  $\delta$  we have no informations whatsoever. Two additional discrete unknowns are the sign of the atmospheric mass difference and the  $\theta_{23}$ -octant (if  $\theta_{23} \neq 45^{\circ}$ ).

The full understanding of the leptonic mixing matrix constitutes, together with the discrimination of the Dirac/Majorana character and the measure of its absolute mass scale, the main neutrino-physics goal for the next decade. However, strong correlations between  $\theta_{13}$  and  $\delta$  [8] and the presence of parametric degeneracies in the  $(\theta_{13}, \delta)$  parameter space, [9]-[12], make the simultaneous measurement of the two variables extremely difficult. Several setups have been proposed to face these problems and perform this task, the first option being Super-Beam's (of which T2K [13] is the first approved one). New machines have been also proposed, such as the  $\beta$ -Beam [14] or the Neutrino Factory [15].

In the literature, however, the simultaneous measurement of  $\theta_{13}$  and  $\delta$  has been normally studied considering the solar and atmospheric mixing parameters as external quantities fixed to their best fit values (see for example Ref. [16] and refs. therein; see also [17] for some recent papers). This is clearly an approximation that has been adopted to get a first insight on the problems related to the  $(\theta_{13}, \delta)$  measurement. However, the experimental uncertainties on these parameters can in principle affect the measurement of the unknowns, and it seems important to perform an analysis that goes beyond the two-parameters fits presented in the literature.

In this paper we therefore study, in a systematic way, the impact that "solar" (i.e.  $\theta_{12}$  and  $\Delta m_{sol}^2$ ) and "atmospheric" (i.e.  $\theta_{23}$  and  $\Delta m_{atm}^2$ ) parameters uncertainties have on the measurement of  $\theta_{13}$  and  $\delta$  at three of the many proposed setups. By doing this we want to catch the characteristic features of the inclusion of external parameters uncertainties in a  $(\theta_{13}, \delta)$  measurement. A complete six-dimensional fit <sup>2</sup> requires a really hard computing effort. Our approach, conversely, consists of a series of three-parameters fits (taking  $\theta_{12}, \Delta m_{sol}^2, \theta_{23}$  and  $\Delta m_{atm}^2$  in turn as the third fitting variable)

<sup>&</sup>lt;sup>1</sup> A third mass difference,  $\Delta m_{LSND}^2 \sim 1 \text{ eV}^2$ , suggested by the LSND experiment [2], has not being confirmed yet [3] and will not be considered in this paper.

<sup>&</sup>lt;sup>2</sup> To which one could add in principle other variables such as the matter parameter or systematic errors, [18,19].

to be compared with standard two-parameters fits in  $\theta_{13}$  and  $\delta$ . In this way, we realized that the atmospheric parameters are the external inputs whose uncertainties are more important in the reconstruction of  $(\theta_{13}, \delta)$ , and that must be better measured in future experiments. We have also tried to compare our results with other methods that have been proposed to deal with external parameter uncertainties in the measurement of  $\theta_{13}$  and  $\delta$  such as the inclusion of a covariance matrix in two-parameters  $\chi^2$ 's [9] or the so-called CP-coverage [18].

We consider here, as exemplificative setups, three CERN-based facilities:

- the 4 MWatt SPL Super-Beam [20] and a  $\gamma \sim 100~\beta$ -Beam [21] both aimed at the Fréjus tunnel where a 440 kT fiducial volume UNO-like Water Čerenkov detector [22] could be located with a  $L=130~\mathrm{km}$  baseline.
- the CERN-based 50 GeV Neutrino Factory (see Ref. [16] and refs. therein), with two detectors of different characteristics to take advantage of both the "golden" [8] and "silver" [23] channels  $\nu_e \to \nu_\mu, \nu_\tau$ . The two detectors considered are a 40 kT magnetized iron detector [24] located at L=3000 km and a 4 kT emulsion cloud chamber [25] located at L=732 km in the Gran Sasso tunnel.

By comparing the results at these three, very different, facilities, we deduce that the impact of the atmospheric parameters uncertainties is a common problem that future experiments looking for  $\theta_{13}$  and  $\delta$  will have to face. We do not repeat our analysis for all of the setups that have been proposed. It is our belief that, at this level of the discussion on future facilities, it is more relevant to address the problem of how uncertainties in the atmospheric and solar parameters affect the measurement of  $(\theta_{13}, \delta)$  at setups that have been thoroughly discussed than to present a comprehensive comparison between two- and three-parameters fits at all of the facilities proposed in the literature.

The paper is organized as follows: in Sect. 2 we shortly introduce the three facilities and the neutrino-nucleon cross-section; in Sect. 3 we remind the central values and the uncertainties of solar and atmospheric parameters; in Sect. 5 we review the parametric degeneracies in the measurement of  $\theta_{13}$  and  $\delta$  in appearance and disappearance channels; in Sect. 4 we introduce the statistical approach used in the paper; in Sect. 6 we present our results for the measurement of  $\theta_{13}$  and  $\delta$  taking into account the uncertainties on solar and atmospheric parameters; in Sect. 7 we show the CP-violation discovery potential of the considered facilities taking into account the uncertainties on atmospheric parameters; in Sect. 8 we eventually draw our conclusions. In App. A we compare our statistical approach with other methods; in App. B we present three-parameters fits for the three considered setups for different choices of the input pair  $(\bar{\theta}_{13}, \bar{\delta})$ .

#### 2 The experimental setup

In this section we describe, briefly, the three facilities that we will use in the following and we remind the neutrino-nucleon cross-section used throughout the paper.

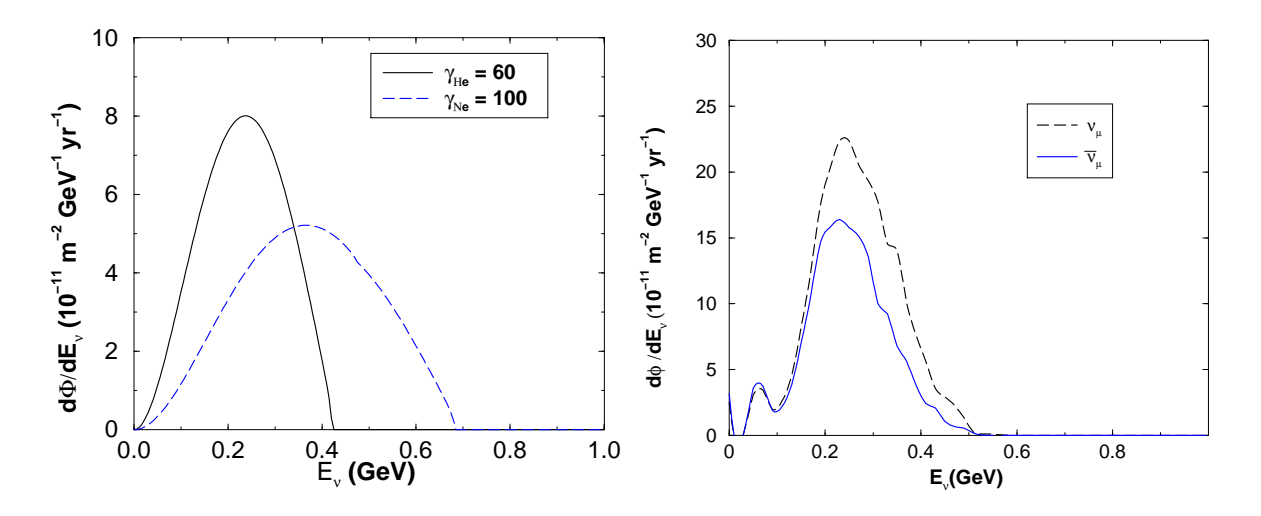


Fig. 1. Left:  $\beta$ -Beam fluxes at the Fréjus location (L = 130 km) [27]; Right: SPL Super-Beam fluxes at the Fréjus location (130 km baseline) [34].

## 2.1 The $\beta$ -Beam

The  $\beta$ -Beam concept was first introduced in Ref. [14]. It involves producing a beam of  $\beta$ -unstable heavy ions, accelerating them to some reference energy, and allowing them to decay in the straight section of a storage ring, resulting in a very intense neutrino beam. The chosen ions are  ${}^6{\rm He}$ , to produce a pure  $\bar{\nu}_e$  beam, and  ${}^{18}{\rm Ne}$ , to produce a  $\nu_e$ beam. We follow the setup proposed in Ref. [21]: the  $\gamma$  ratio for the two ions has been fixed to  $\gamma(^6\text{He})/\gamma(^{18}\text{Ne}) = 3/5$ , in order to have both ions circulating in the storage ring at the same time; the  $\gamma$  value has been fixed to  $\gamma_{^{18}\mathrm{Ne}} = 100$  (i.e.,  $\gamma_{^{6}\mathrm{He}} = 60$ ) to tune the neutrino/antineutrino mean energy at the maximum of the  $\nu_e \to \nu_\mu$  oscillation probability for the CERN to Fréjus baseline. A flux of 2.9×10<sup>18</sup> <sup>6</sup>He decays/year and  $1.1 \times 10^{18}$  <sup>18</sup>Ne decays/year is assumed. Fig. 1(left) shows the  $\beta$ -Beam neutrino fluxes computed at L=130 km, keeping  $m_e \neq 0$  [26] and taking into account the three different decay modes of <sup>18</sup>Ne [27]. The mean energy of the  $\overline{\nu}_e$ ,  $\nu_e$  beams for this setup is 0.23 GeV and 0.37 GeV, respectively. Clearly, energy resolution is very poor at such low energy, given the influence of Fermi motion and other nuclear effects. Therefore, in the following all the sensitivities are computed for a counting experiment with no energy cuts [28]. The  $\beta$ -Beam is a clean environment to produce electron-type neutrinos: the main sources of systematic error are the overall flux normalization (that can be controlled with a near detector), the definition of the fiducial volume of the detector and the neutrino-nucleon cross-sections. Alternative  $\beta$ -Beam proposals can be found in Refs. [26,29,30,19].

#### 2.2 The Super-Beam

A Super-Beam is a conventional neutrino beam with a proton intensity higher than that of existing (or under construction) beams such as K2K [31], NuMI [32] and the

CNGS [33]. With respect to the  $\beta$ -Beam and the Neutrino Factory, neutrino beams of a new design, it has the advantage of a well known technology. On the other hand, the flux composition (with  $\nu_{\mu}$  as the main component for a  $\pi^+$  focusing, plus a small but unavoidable admixture of  $\bar{\nu}_{\mu}$ ,  $\nu_{e}$  and  $\bar{\nu}_{e}$ ) limits its sensitivity to  $\nu_{\mu} \to \nu_{e}$  oscillations.

We follow the setup proposed in Ref. [20] as a reference: a 2.2 GeV proton beam of 4 MWatt power (the SPL), with neutrino fluxes computed in a full simulation of the beamline in Ref. [34], assuming a decay tunnel length of 60 m. The corresponding fluxes are shown in Fig. 1(right). Notice that this beam was designed, originally, as the first stage of a would-be Neutrino Factory, and it has not been optimized as a facility to look for  $\nu_{\mu} \rightarrow \nu_{e}$  on its own. Such an optimization has been presented in Ref. [35]. Also in this case, as it was for the  $\beta$ -beam, the main source of systematic error are the poorly known neutrino-nucleon cross-sections, the definition of the fiducial volume in the far detector and the overall normalization of the flux (with the additional problem of new background coming from neutrino species not present in the  $\beta$ -Beam flux). For this setup, also, we consider two tentative values of systematic error: an "optimistic" 5%.

#### 2.3 The Neutrino Factory

The Neutrino Factory that we consider consists of a SPL-like Super-Beam and a 50 GeV muon storage ring [36], with  $2 \times 10^{20}$  muons decaying in the straight section of the storage ring per year. Five years of data taking for each muon polarity is envisaged. Two detectors of different technology are considered: a 40 kT Magnetized Iron Detector (MID) at L=2810 km; and a 4 kT Emulsion Cloud Chamber (ECC) at L=732 or 2810 km. This proposal corresponds to the design of a possible CERN-based Neutrino Factory Complex, with detectors located at the Gran Sasso Laboratory (the ECC) and at a second site to be defined (the MID and possibly the ECC). Each one of these detectors is especially optimized to look for a particular signal: the "golden" channel  $\nu_e \to \nu_\mu$  for the 40 kT MID, and the "silver" channel  $\nu_e \to \nu_\tau$  for the 4 kT ECC. The corresponding neutrino fluxes are shown in Fig. 2(left).

The detectors background and systematics for this specific facility have been studied in details in Ref. [24] (the Magnetized Iron Calorimeter) and in Ref. [25] (the Emulsion Cloud Chamber).

#### 2.4 The neutrino cross-section

An important source of systematic error is our present poor knowledge of the  $\nu N$  and  $\bar{\nu}N$  cross-sections for energies below 1 GeV [37]: either there are very few data (the case of neutrinos) or there are no data at all (the case of antineutrinos). On top of that, the few available data have generally not been taken on the target used in the experiments (either water, iron or lead), and the extrapolation from different nuclei is

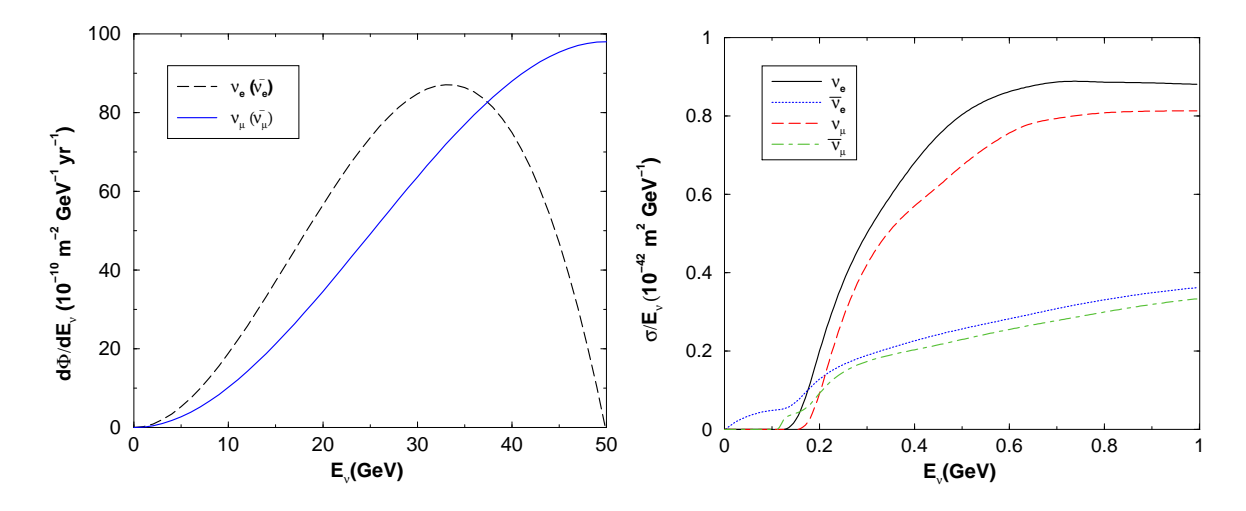


Fig. 2. Left: 50 GeV Neutrino Factory fluxes at the Gran Sasso location (L=732 km) [8]; Right:  $\nu N$  and  $\bar{\nu} N$  cross-sections on water [38].

complicated by nuclear effects that at the considered energies play an important role. For definiteness we show in Fig. 2(right) the cross-sections on water used for the Water Čerenkov detector throughout the paper [38]. Notice that we also used cross-sections on iron and lead for the MID and the ECC, respectively.

## 3 The leptonic mixing parameters

In Tab. 1 we remind the values of solar and atmospheric sector parameters used in the paper, their present uncertainties and the errors expected after a round of new experiments.

In particular, in the second column of Tab. 1 we report the input values for  $\theta_{12}, \theta_{23}, \Delta m_{atm}^2$  and  $\Delta m_{sol}^2$  used in the paper. They correspond to the present best fit values for solar and atmospheric parameters [39] with the only exception of  $\theta_{23}$ , for which we do not use the present best fit value,  $\theta_{23}=45^\circ$ , but  $\theta_{23}=40^\circ$  to make manifest the impact of possible octant degeneracies on the results [11]. Notice that throughout the paper the experimentally measured atmospheric mass difference (whose present best fit value will be labelled as  $\Delta m_{atm}^2$ ) will be fitted with the three-family parameter  $|\Delta m_{23}^2| = |m_3^2 - m_2^2|$  (see [40] for a different convention). For the solar mass difference, on the other hand, we can unambiguously identify the three-family parameter  $\Delta m_{12}^2 = m_2^2 - m_1^2$  with the experimentally measured quantity,  $\Delta m_{sol}^2$ . In the third column of Tab. 1 we report the present uncertainties on each of the parameters. Finally, in the fourth column, we present the uncertainties on solar and atmospheric parameters that are expected to be achieved with ongoing or planned experiments. For an estimate of the reduction of solar parameter uncertainties we refer to Ref. [41]. For an estimate of the reduction of atmospheric parameter uncertainties we refer to the Letter of Intent of the T2K-phase I experiment, [13]. The expected error on  $|\Delta m_{23}^2|$  for the central value  $|\Delta m_{23}^2| = \Delta m_{atm}^2 = 2.5 \times 10^{-3} \text{ eV}^2$  is a function of the sign of the atmospheric mass

difference, something that will not be measured at T2K-I. For this reason we present both spreads specifying the chosen hierarchy, using the results of an analysis yet to appear, [42].

The T2K-I improved bounds are used to analyse the impact of the expected atmospheric uncertainties in the measurement of  $(\theta_{13}, \delta)$  at the  $\beta$ -Beam and the Neutrino Factory<sup>3</sup>. On the other hand, in Sect. 5.2 it will be shown that the  $\nu_{\mu}$  disappearance channel at the SPL Super-Beam can improve significantly the present uncertainties on the atmospheric parameters. This measure will therefore be combined with the appearance channel when analysing the impact of the atmospheric uncertainties in the measure of  $(\theta_{13}, \delta)$  at the Super-Beam.

Solar Sector	Central values	Present [39]	Expected (KamLand) [41]
$\tan^2 \theta_{12}$	0.39	0.30 - 0.54	0.30 - 0.51
$\Delta m^2_{12}~({\rm eV^2})$	$8.2 \times 10^{-5}$	$(7.5 - 9.1) \times 10^{-5}$	$(7.7 - 8.7) \times 10^{-5}$
Atmospheric Sector	Central values	Present [39]	Expected (T2K-phaseI) [42]
$\tan^2 \theta_{23}$	0.7	0.53 - 2.04	0.62 - 0.85 / 1.21 - 1.66
$ \Delta m_{23}^2  \ (\mathrm{eV}^2)$	$2.5 \times 10^{-3}$	$(1.7 - 3.5) \times 10^{-3}$	$s_{atm} = +, (2.42 - 2.61) \times 10^{-3}$
			$s_{atm} = -, (2.46 - 2.64) \times 10^{-3}$
			Expected (SPL, this paper)
$\tan^2 \theta_{23}$	0.7	0.53 - 2.04	0.53 - 2.04
$ \Delta m_{23}^2  \; ({\rm eV}^2)$	$2.5\times10^{-3}$	$(1.7 - 3.5) \times 10^{-3}$	$s_{atm} = +, (2.30 - 2.75) \times 10^{-3}$
			$s_{atm} = -, (2.40 - 2.90) \times 10^{-3}$

Table 1

Central values and allowed ranges for solar and atmospheric parameters.

## 4 Statistical approach

In this section we describe the statistical approach used in the paper to estimate the impact of uncertainties in the atmospheric and solar parameters in the measurement of  $(\theta_{13}, \delta)$ .

The obvious approach would be to fit the data in  $(N_{\alpha} + 2)$  parameters, with  $N_{\alpha}$  the number of external parameters that are allowed to vary in a given range (e.g., the solar and atmospheric parameters plus the matter density). This procedure, however, is increasingly time-consuming as the number of parameters to be fitted goes up. For

<sup>&</sup>lt;sup>3</sup> An updated detailed computation of the expected errors on atmospheric parameters that can be obtained at this facility is lacking, [43,44].

this reason, in order to understand how any single parameter affect the measurement, we perform three-parameters fits in  $\theta_{13}$ ,  $\delta$  and one of the following parameters in turn:  $\theta_{12}$ ,  $\Delta m_{12}^2$ ,  $\theta_{23}$  and  $\Delta m_{23}^2$ . The matter density has been considered as a fixed quantity throughout the paper [45].

To perform the three-parameters fits we have constructed grids for the expected number of charged-current events for each facility, each grid in the two unknowns,  $\theta_{13}$  and  $\delta$ , plus the two measured parameters in the solar sector  $(\theta_{12}, \Delta m_{sol}^2)$  or in the atmospheric sector  $(\theta_{23}, \Delta m_{23}^2)$ . When studying the impact of solar parameter uncertainties we have fixed the atmospheric parameters to  $\theta_{23} = 40^{\circ}$  and  $\Delta m_{23}^2 = 2.5 \times 10^{-3}$  eV<sup>2</sup> and computed four different grids, for  $s_{atm} = \pm 1$ ;  $s_{oct} = \pm 1$ . When studying the impact of atmospheric parameter uncertainties we have fixed the solar parameters to  $\theta_{12} = 32^{\circ}$  and  $\Delta m_{sol}^2 = 8.2 \times 10^{-5}$  eV<sup>2</sup>. In this case, only two grids must be computed, one for each value of  $s_{atm}$ : the octant-degeneracy need not to be considered as an external (discrete) input, since  $\theta_{23}$  is one of the free parameters in the grid.

When a three-parameters fit is performed, the other parameters in the grid are fixed to the corresponding present best fit value for  $\theta_{12}$ ,  $\Delta m_{sol}^2$  and  $\Delta m_{23}^2$  or to  $\theta_{23} = 40^\circ$  for the atmospheric angle (to take into account possible octant and mixed degeneracies, that would disappear for maximal mixing). This procedure is used to study the effect of one parameter at a time on the  $(\theta_{13}, \delta)$  measure. The  $\chi^2$  function is:

$$\left[\chi^2(\theta_{13}, \delta, x)\right]_{\alpha\beta} = \sum_{\pm} \left[ \frac{N_{\alpha\beta}^{\pm}(\theta_{13}, \delta, x; s_{atm}, s_{oct}) - N_{\alpha\beta}^{\pm}(\bar{\theta}_{13}, \bar{\delta}, \bar{x}; \bar{s}_{atm}, \bar{s}_{oct})}{\delta N_{\alpha\beta}^{\pm}} \right]^2, \quad (1)$$

with x any of the parameters to be fitted in addition to  $\theta_{13}$  and  $\delta$ ,  $\pm$  refers to neutrinos or antineutrinos and  $N_{\alpha\beta}^{\pm}$  is the number of charged leptons  $l_{\beta}^{\pm}$  observed in the detector for a  $\nu_{\alpha}(\bar{\nu}_{\alpha})$  beam. The error on the sample  $N_{\alpha\beta}^{\pm}$  is:

$$(\delta N_{\alpha\beta}^{\pm})^2 = \sigma_{N_{\alpha\beta}^{\pm}}^2 + (\epsilon_{\beta}^{\pm} N_{\alpha\beta}^{\pm})^2 + (\epsilon_{\beta}^{\pm} B_{\alpha\beta}^{\pm})^2, \qquad (2)$$

where  $\sigma_{N_{\alpha\beta}^{\pm}}$  is the statistical error on  $N_{\alpha\beta}^{\pm}$  (Gaussian or Poissonian, depending on the corresponding statistics),  $B_{\alpha\beta}^{\pm}$  is the sum of beam and detector backgrounds for the considered channel, computed as in Refs. [20,21], and  $\epsilon_{\beta}^{\pm}$  is the total systematic error for the considered channel at a given facility. No covariance matrix for the non-fitted parameters has been considered. The three-parameters  $\chi^2$  function defines a three-dimensional 90% CL contour that is eventually projected onto the  $(\theta_{13}, \delta)$  plane to perform a direct comparison with the standard two-parameters 90% CL contours for the considered setups  $^4$  [21,26,27].

A discussion on the statistical approach chosen and its difference with existing approaches [9,18] is mandatory and can be found in App. A.

<sup>&</sup>lt;sup>4</sup> A preliminary result obtained by means of this procedure has been presented in [46].

#### 5 Parameter correlations and degeneracies

Parameter correlations and degeneracies arise in the determination of  $\theta_{13}$  and  $\delta$  at future neutrino experiments, as it has been studied in many papers [9]-[12]. The problem is due to the strong correlation between these two parameters in the appearance transition probabilities ( $\nu_e \to \nu_\mu, \nu_\tau$  and  $\nu_\mu \to \nu_e$ ) and in the present (and near future) ignorance of two discrete unknowns, the sign of the atmospheric mass difference  $\Delta m_{23}^2$  and the  $\theta_{23}$ -octant, that can be parametrized by the sign variables  $s_{atm} = \text{sign}[\Delta m_{23}^2]$  and  $s_{oct} = \text{sign}[\tan(2\theta_{23})]$  that take the values  $\pm 1$  for  $\Delta m_{23}^2 > 0 (<0)$  and  $\theta_{23} < 45^{\circ} (>45^{\circ})$ , respectively. Solving the systems of equations corresponding to the four distinct choices of  $s_{atm}$  and  $s_{oct}$ :

$$N_{\alpha\beta}^{\pm}(\bar{\theta}_{13}, \bar{\delta}; \bar{s}_{atm}, \bar{s}_{oct}) = N_{\alpha\beta}^{\pm}(\theta_{13}, \delta; s_{atm} = \bar{s}_{atm}; s_{oct} = \bar{s}_{oct}), \qquad (3)$$

$$N_{\alpha\beta}^{\pm}(\bar{\theta}_{13}, \bar{\delta}; \bar{s}_{atm}, \bar{s}_{oct}) = N_{\alpha\beta}^{\pm}(\theta_{13}, \delta; s_{atm} = -\bar{s}_{atm}, s_{oct} = \bar{s}_{oct}), \qquad (4)$$

$$N_{\alpha\beta}^{\pm}(\bar{\theta}_{13}, \bar{\delta}; \bar{s}_{atm}, \bar{s}_{oct}) = N_{\alpha\beta}^{\pm}(\theta_{13}, \delta; s_{atm} = \bar{s}_{atm}, s_{oct} = -\bar{s}_{oct}), \qquad (5)$$

$$N_{\alpha\beta}^{\pm}(\bar{\theta}_{13}, \bar{\delta}; \bar{s}_{atm}, \bar{s}_{oct}) = N_{\alpha\beta}^{\pm}(\theta_{13}, \delta; s_{atm} = -\bar{s}_{atm}, s_{oct} = -\bar{s}_{oct}), \tag{6}$$

(with  $N_{\alpha\beta}^{\pm}$  defined in the previous section) will result, in general, in the input pair  $(\bar{\theta}_{13}, \bar{\delta})$  plus seven additional solutions (the *clones*) to form an eightfold degeneracy: the *intrinsic clone* (Eq. 3), the *sign clones* (Eq. 4), the *octant clones* (Eq. 5) and the *mixed clones* (Eq. 6). A complete theoretical analysis of the clones location has been presented in Ref. [47], where an algorithm to numerically find each clone location in the  $(\theta_{13}, \delta)$  plane as a function of the considered experimental setup and of the input parameters has been given. A similar approach can be applied to study the presence of degeneracies in the disappearance channels  $\nu_e \to \nu_e$  and  $\nu_\mu \to \nu_\mu$ .

#### 5.1 Correlation and degeneracies in $\nu_e$ disappearance

The  $\nu_e$  disappearance probability does not depend on the CP violating phase  $\delta$  and on the atmospheric  $\theta_{23}$  mixing angle. The  $\theta_{13}$  measurement is, therefore, not affected by  $(\theta_{13} - \delta)$  correlations nor by the  $s_{oct}$  ambiguity. The  $\nu_e \to \nu_e$  matter oscillation probability, expanded at second order in the small parameters  $\theta_{13}$  and  $(\Delta m_{sol}^2 L/E)$  reads:

$$P_{ee}^{\pm} = 1 - \left(\frac{\Delta_{23}}{B_{\mp}}\right)^2 \sin^2(2\theta_{13}) \sin^2\left(\frac{B_{\mp}L}{2}\right) - \left(\frac{\Delta_{12}}{A}\right)^2 \sin^2(2\theta_{12}) \sin^2\left(\frac{AL}{2}\right) , \tag{7}$$

where  $\Delta_{23} = \Delta m_{23}^2/2E$ ,  $\Delta_{12} = \Delta m_{12}^2/2E$ ,  $A = \sqrt{2}G_FN_e$  and  $B_{\mp} = |A \mp \Delta_{atm}|$  with  $\pm$  for neutrinos (antineutrinos), respectively. This formula describes reasonably well the behaviour of the transition probability in the energy range covered by the considered

 $\beta$ -Beam setup ( $L \sim 100$  km and  $E_{\nu} \sim 100$  MeV) and it illustrates clearly that two sources of ambiguities are still present in  $\nu_e$  disappearance,  $s_{atm}$  (for large values of  $\theta_{13}$ , i.e. in the "atmospheric" region) and the ( $\theta_{13} - \theta_{12}$ ) correlation (for small values of  $\theta_{13}$ , i.e. in the "solar" region). A  $\beta$ -Beam could in principle improve our present errors on the solar parameters through  $\nu_e$  disappearance. We have checked that this is not the case for the considered setup: at large  $\theta_{13}$  the second term in eq. (7) dominates over the last term, that is more sensitive to solar parameters. On the other hand, for small  $\theta_{13}$  the statistics is too low to improve present uncertainties on  $\theta_{12}$  and  $\Delta m_{sol}^2$  (remind that energy and baseline of the low- $\gamma$   $\beta$ -Beam has not been chosen to fulfill this task, and therefore our results are not surprising at all). Eventually, in Ref. [48] it has been shown that if systematic errors cannot be controlled better than at 5%, the  $\beta$ -Beam disappearance channel does not improve the CHOOZ bound on  $\theta_{13}$ .

Eq. (7) can be also applied to reactor experiments aiming to a precise measurement of  $\theta_{13}$  in a "degeneracy-free" environment. For the typical baseline and energy of a reactor experiment (e.g., L=1.05 km and  $\langle E_{\nu} \rangle = 4$  MeV for the Double-Chooz proposal, [49]) we can safely consider antineutrino propagation in vacuum. As a consequence, no sensitivity to  $s_{atm}$  is expected at these experiments, since  $B_{\mp} \to \Delta_{23}$  for  $\Delta_{23} \gg A$ . It is very difficult that reactor experiments could test small values of  $\theta_{13}$ , and thus the  $\theta_{13} - \theta_{12}$  correlation (significant only in the "solar" region) can also be neglected.

## 5.2 Correlation and degeneracies in $\nu_{\mu}$ disappearance

A Super-Beam facility can perform an independent measurement of the atmospheric parameters via the  $\nu_{\mu}$  disappearance channel: these kind of facilities should in principle reduce the error on the atmospheric mass difference to less than 10 % and on the atmospheric angle to  $\sim 10$  % [50]. It is thus interesting to study, as for the  $\nu_e$  disappearance channel, the presence of parameter correlations and degeneracies. The vacuum oscillation probability expanded to the second order in the small parameters  $\theta_{13}$  and  $(\Delta_{sol}L/E)$  [51] is:

$$P(\nu_{\mu} \to \nu_{\mu}) = 1 - \left[ \sin^{2} 2\theta_{23} - s_{23}^{2} \sin^{2} 2\theta_{13} \cos 2\theta_{23} \right] \sin^{2} \left( \frac{\Delta_{23}L}{2} \right)$$

$$- \left( \frac{\Delta_{12}L}{2} \right) \left[ s_{12}^{2} \sin^{2} 2\theta_{23} + \tilde{J}s_{23}^{2} \cos \delta \right] \sin(\Delta_{23}L)$$

$$- \left( \frac{\Delta_{12}L}{2} \right)^{2} \left[ c_{23}^{4} \sin^{2} 2\theta_{12} + s_{12}^{2} \sin^{2} 2\theta_{23} \cos(\Delta_{23}L) \right],$$
(8)

where  $\tilde{J} = \cos \theta_{13} \sin 2\theta_{12} \sin 2\theta_{13} \sin 2\theta_{23}$ . The first term in the first parenthesis is the dominant one and is symmetric under  $\theta_{23} \to \pi/2 - \theta_{23}$ . This is indeed the source of our present ignorance on  $s_{oct}$ . This symmetry is lifted by the other terms, that introduce a mild CP-conserving  $\delta$ -dependence also, albeit through subleading effects very difficult to isolate. We present our results for the  $\nu_{\mu}$  disappearance channel in the  $(\theta_{23}, \Delta m_{23}^2)$ 

plane: as a consequence, we do not need to specify the  $\theta_{23}$ -octant, since the interval  $\theta_{23} \in [35^{\circ}, 55^{\circ}]$  is spanned explicitly.

Solving the two systems of equations:

$$N_{\mu\mu}^{\pm}(\bar{\theta}_{23}, \Delta m_{atm}^2; \bar{s}_{atm}) = N_{\mu\mu}^{\pm}(\theta_{23}, |\Delta m_{23}^2|; \bar{s}_{atm}), \qquad (9)$$

$$N_{\mu\mu}^{\pm}(\bar{\theta}_{23}, \Delta m_{atm}^2; \bar{s}_{atm}) = N_{\mu\mu}^{\pm}(\theta_{23}, |\Delta m_{23}^2|; -\bar{s}_{atm}), \qquad (10)$$

four different solutions are found for  $\bar{\theta}_{23} \neq 45^{\circ}$ : two solutions from eq. (9), the input value  $\theta_{23} = \bar{\theta}_{23}$  and  $\theta_{23} \simeq \pi/2 - \bar{\theta}_{23}$ , being the second solution not exactly at  $\theta_{23} = \pi/2 - \bar{\theta}_{23}$  due to the small  $\theta_{23}$ -octant asymmetry; and two more solutions from eq. (10) at a different value of  $|\Delta m_{23}^2|$  [48]. In eq. (8) we can see that changing sign to  $\Delta m_{23}^2$  the second term becomes positive: a change that must be compensated with an increase in  $|\Delta m_{23}^2|$  to give  $P_{\mu\mu}^{\pm}(\Delta m_{atm}^2; \bar{s}_{atm}) = P_{\mu\mu}^{\pm}(|\Delta m_{23}^2|; -\bar{s}_{atm})$ . The two solutions of eq. (10) corresponding to the wrong choice of  $s_{atm}$  can be observed in Fig. 3(left), where equal-number-of-events (ENE) curves are computed for both  $s_{atm} = \bar{s}_{atm}$  (solid) and  $s_{atm} = -\bar{s}_{atm}$  (dotted) at the considered Super-Beam facility. The two intersections are notably off the input pair  $\bar{\theta}_{23} = 40^{\circ}$ ,  $\Delta m_{23}^2 = \Delta m_{atm}^2$ . As expected, the two sign clones are located at  $|\Delta m_{23}^2| \geq \Delta m_{atm}^2$  and are almost symmetric with respect to  $\theta_{23} = 45^{\circ}$ . The shift in the vertical axis is a function of  $\theta_{13}$  and  $\delta$ . If  $\bar{\theta}_{23} = 45^{\circ}$  only two solutions (corresponding to different choices of  $s_{atm}$ ) are expected.

We must also stress that such an uncertainty can be enhanced once we take into account that  $\theta_{13}$  and  $\delta$  are completely unknown [50] (although the impact of this last parameter in  $\nu_{\mu}$  disappearance is expected to be rather small). To gain some feeling on the precision that can be expected in a  $\nu_{\mu}$  disappearance measurement at the SPL Super-Beam facility, we performed a full three-parameters analysis in  $\theta_{23}$ ,  $|\Delta m_{23}^2|$  and  $\theta_{13}$  for the input parameters  $\bar{\theta}_{23} = 40^{\circ}$ ,  $\Delta m_{23}^2 = 2.5 \times 10^{-3}$  eV<sup>2</sup> and  $\bar{\theta}_{13} = 7^{\circ}$ . We have then projected the 90% three-parameters CL contour onto the  $(\theta_{23}, |\Delta m_{23}^2|)$  plane, Fig. 3(right). In the absence of a complete simulation of the systematics and the background for the  $\nu_{\mu}$  disappearance channel at the SPL Super-Beam [20], we have adopted as an estimate of the expected background and efficiency those used in [21,26] and [27] for the  $\nu_{e} \rightarrow \nu_{\mu}$  appearance channel at the  $\beta$ -Beam facility. A 2% systematic error has been assumed. The solid line refers to the projection of the three-dimensional 90 % CL contour on the  $(\theta_{23}, |\Delta m_{23}^2|)$  plane for  $s_{atm} = \bar{s}_{atm}$ , the dotted line to the projection of the 90 % CL contour for  $s_{atm} = -\bar{s}_{atm}$ .

As expected, the three-parameters fit presents a second allowed region in the parameter space at  $|\Delta m^2_{23}| > \Delta m^2_{atm}$  when the wrong  $s_{atm}$  is considered. Notice that, performing a three-parameters fit in  $\theta_{23}$ ,  $\Delta m^2_{23}$  and  $\delta$ , the difference between the two- and three-parameters contours is much smaller. In [48] it has been shown that a larger spread in  $\theta_{23}$  is found for  $\bar{\theta}_{23} \neq 45^{\circ}$ . We can perform fits with  $\theta_{23}$  non-maximal and for different input values for  $\bar{\theta}_{13} \in [0, 10^{\circ}]$ . The result of such an analysis is that the SPL Super-Beam will be able to measure  $\theta_{23}$  in the interval  $[36^{\circ}, 55^{\circ}]$  and  $\Delta m^2_{23}$  in  $[2.3, 2.9] \times 10^{-3} \, \mathrm{eV}^2$ 

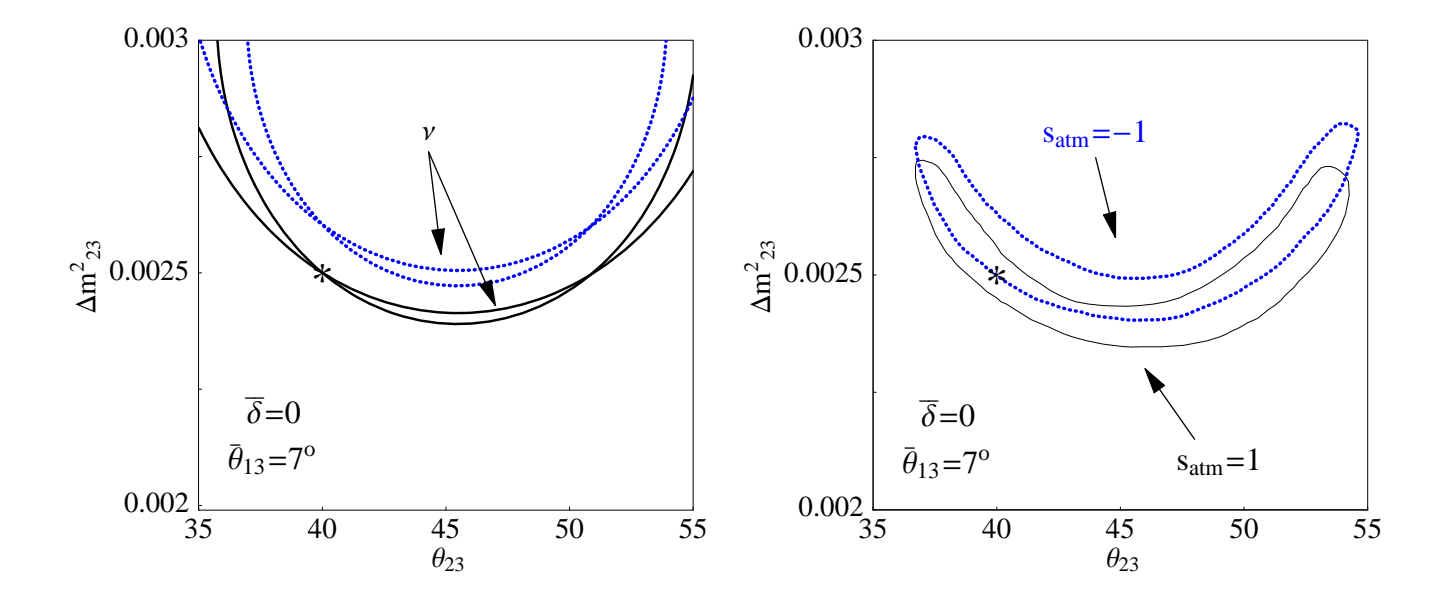


Fig. 3. Left: ENE curves in the  $(\theta_{23}, |\Delta m_{23}^2|)$  plane at the SPL Super-Beam facility, for  $s_{atm} = \bar{s}_{atm}$  (solid) and  $s_{atm} = -\bar{s}_{atm}$  (dotted) and  $\bar{\theta}_{23} = 40^{\circ}$ ,  $\Delta m_{atm}^2 = 2.5 \times 10^{-3}$  eV<sup>2</sup>. Right: Projection of the three-parameters 90 % CL contour in  $(\theta_{23}, |\Delta m_{23}^2|, \theta_{13})$  at the Super-Beam facility for the input point  $\bar{\theta}_{23} = 40^{\circ}$ ,  $\Delta m_{atm}^2 = 2.5 \times 10^{-3}$  eV<sup>2</sup> and  $\bar{\theta}_{13} = 7^{\circ}$  onto the  $(\theta_{23}, |\Delta m_{23}^2|)$  plane. Again, the solid (dotted) line stands for  $s_{atm} = \bar{s}_{atm}$  ( $s_{atm} = -\bar{s}_{atm}$ ).

for the input pair  $\bar{\theta}_{23} = 40^{\circ}$ ,  $\Delta m_{23}^2 = \Delta m_{atm}^2$ . Notice that the expected SPL precision on  $\Delta m_{23}^2$  is comparable with what expected at T2K-I [13]. On the other hand, the expected SPL precision on  $\theta_{23}$  is much worse than the T2K-I one, a consequence of the fact that the considered SPL setup is a counting experiment and it has no energy resolution.

## 6 Impact of parameter uncertainties on $\theta_{13}$ and $\delta$

In this section, we discuss the impact of the uncertainties in the solar and atmospheric parameters to the simultaneous measurement of  $\theta_{13}$  and  $\delta$  at the considered  $\beta$ -Beam, Super-Beam and Neutrino Factory. The three experiments will be discussed separately. In all fits we have combined informations from all available channels for both polarities,

$$\chi^{2}(\theta_{13}, \delta, x) = \sum_{i} \chi_{i}^{2}(\theta_{13}, \delta, x), \qquad (11)$$

where  $\chi_i^2$  is the three-parameters  $\chi^2$  function defined as in eq. (1) for a given channel and polarity. All channels have been taken as independent measurement and no covariance matrix has been introduced, following the approach described in Sect. 4. In general, a "pessimistic" systematic error,  $\epsilon^{\pm} = 5\%$ , has been used in appearance channels. On

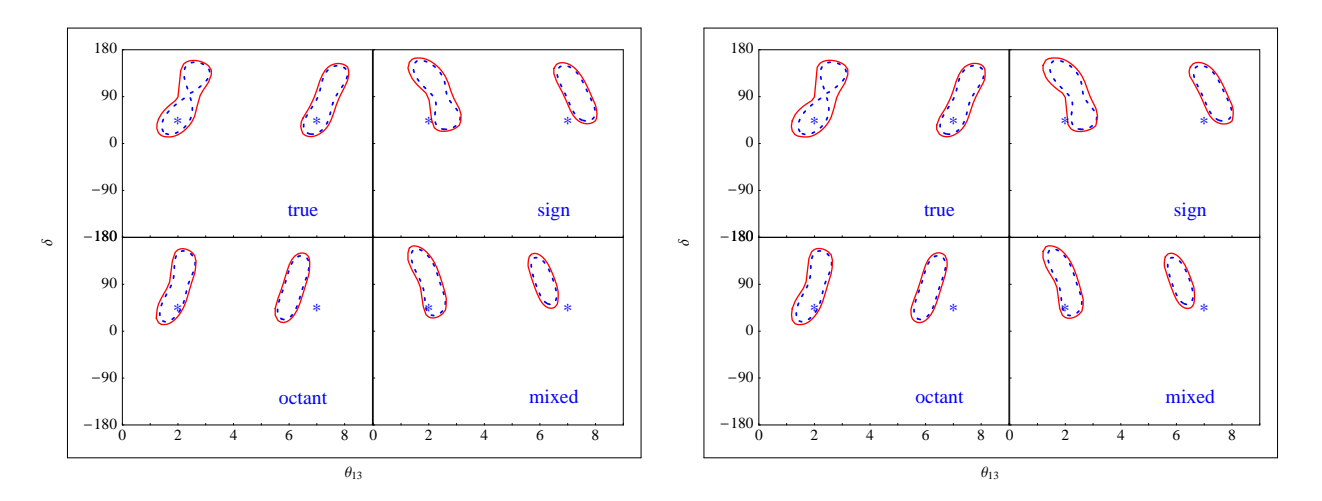


Fig. 4. Comparison of the projection of three-parameters 90% CL contours onto the  $(\theta_{13}, \delta)$  plane (solid lines) with the corresponding two-parameters 90% CL contours (dashed lines) after a 10 years run at the  $\beta$ -Beam. Different choices of  $s_{atm}, s_{oct}$  are plotted separately. The input parameters (represented by a star) are:  $\bar{\theta}_{13} = 2^{\circ}, 7^{\circ}, \ \bar{\delta} = 45^{\circ}$ . Left panel:  $x = \theta_{12}$ ; right panel:  $x = \Delta m_{12}^2$ .

the other hand, a 2% systematic error has been used in disappearance channels.

#### 6.1 The solar sector

We study the effect of present uncertainties on the solar sector parameters in the measurement of  $\theta_{13}$  and  $\delta$  performing two distinct three-parameters fit in  $\theta_{13}$ ,  $\delta$  and  $\theta_{12}$  (for fixed  $\Delta m_{sol}^2$ ) or  $\Delta m_{sol}^2$  (for fixed  $\theta_{12}$ ). The fits have been performed using 10 years of  $\beta$ -Beam running with both polarities.

The projection of the three-parameters 90% CL contours onto the  $(\theta_{13}, \delta)$  plane are presented in Fig. 4. In the left panel we have fixed  $\Delta m_{sol}^2 = 8.2 \times 10^{-5} \text{ eV}^2$  and drawn the projection of the three-dimensional contours for  $\chi^2(\theta_{13}, \delta, \theta_{12})$ , for  $\theta_{12} \in [29^\circ, 36^\circ]$ . In the right panel we have fixed  $\theta_{12} = 32^\circ$  and drawn the projection of the three-dimensional contours for  $\chi^2(\theta_{13}, \delta, \Delta m_{sol}^2)$ , for  $\Delta m_{sol}^2 \in [7.5, 9.1] \times 10^{-5} \text{ eV}^2$ . In both cases, the atmospheric parameters have been fixed to  $\Delta m_{atm}^2 = 2.5 \times 10^{-3} \text{ eV}^2$  and  $\theta_{23} = 40^\circ$ . The input values for the two unknowns are  $\bar{\theta}_{13} = 2^\circ, 7^\circ$  and  $\bar{\delta} = 45^\circ$ . For each panel, the results for the four different choices of the two discrete variables,  $s_{atm}$  and  $s_{oct}$ , are presented separately. Finally, the projection of the three-parameters 90% CL contours (solid lines) are directly compared with the two-parameters 90% CL contours (dashed lines) obtained fixing the solar parameters to their present best fit values,  $\theta_{12} = 32^\circ, \Delta m_{sol}^2 = 8.2 \times 10^{-5} \text{ eV}^2$ .

As we can see in both panels, most of the plotted three-parameters contours coincide for any practical purpose with the corresponding two-parameters ones, with small deviations easily explained by the different CL in two- and three-parameters  $\chi^2$ . As a result, we claim that the impact of solar parameter uncertainties on the measurement

of  $\theta_{13}$  and  $\delta$  is negligible for  $\bar{\theta}_{13} \geq 2^{\circ}$ . This is indeed a consequence of the subleading dependence of the  $\nu_e \to \nu_{\mu}$  oscillation probability on the solar parameters (see, for example, Refs. [8,51]) for large values of  $\bar{\theta}_{13}$ . When  $\bar{\theta}_{13}$  is large, we are in what has been called the "atmospheric regime" in Ref. [9]; only for  $\bar{\theta}_{13}$  below the verge of the  $\beta$ -Beam  $\theta_{13}$ -sensitivity, i.e. for  $\bar{\theta}_{13} > 2^{\circ}$ , we enter in the so-called "solar regime". Clearly, no signal is expected at the  $\beta$ -Beam in this case: we can thus safely claim that the solar parameter uncertainties do not affect significantly the measurement of  $\theta_{13}$  and  $\delta$  at the considered facility.

Similar conclusions can be drawn for the SPL Super-Beam and for different values of  $\bar{\delta}$  and will therefore not be repeated here. For the rest of the paper, the solar parameters will be considered as fixed external inputs:  $\theta_{12} = 32^{\circ}$  and  $\Delta m_{sol}^2 = 8.2 \times 10^{-5} \text{ eV}^2$ .

#### 6.2 The atmospheric sector at the $\beta$ -Beam

As for the solar sector, we study the effect of present uncertainties on the atmospheric sector parameters in the measurement of  $\theta_{13}$  and  $\delta$  performing two distinct three-parameters fit in  $\theta_{13}$ ,  $\delta$  and  $\theta_{23}$  (for fixed  $\Delta m_{23}^2$ ) or  $\Delta m_{23}^2$  (for fixed  $\theta_{23}$ ).

The comparison between two- and three-parameters fits is presented in Fig. 5, where the projection of the three-parameters 90% CL contours onto the  $(\theta_{13}, \delta)$  plane (solid lines) and the two-parameters 90% CL contours (dashed lines) have been plotted separately for each possible choice of the two discrete variables,  $s_{atm}$  and  $s_{oct}$ . In the left panel we have fixed  $\Delta m^2_{atm} = 2.5 \times 10^{-3} \text{ eV}^2$  and drawn the projection of the three-dimensional contours for  $\chi^2(\theta_{13}, \delta, \theta_{23})$ , for  $\theta_{23} \in [36^\circ, 55^\circ]$  (see Tab. 1). In the right panel we have fixed  $\theta_{23} = 40^\circ$  and drawn the projection of the three-dimensional contours for  $\chi^2(\theta_{13}, \delta, \Delta m^2_{23})$ , for  $\Delta m^2_{23} \in [1.7, 3.5] \times 10^{-3} \text{ eV}^2$  (see Tab. 1). The input values for the two unknowns are  $\bar{\theta}_{13} = 2^\circ, 7^\circ$  and  $\bar{\delta} = 45^\circ$ . The two-parameters contours have been drawn using fixed values for the atmospheric parameters,  $\theta_{23} = 40^\circ, \Delta m^2_{atm} = 2.5 \times 10^{-3} \text{ eV}^2$ . We have checked that no significant improvement is observed when the systematic error in the appearance channel is set to 2%.

In Fig. 5 it is manifest the impact of atmospheric parameter uncertainties on the measurement of  $\theta_{13}$  and  $\delta$ , for both  $\theta_{23}$  and  $\Delta m_{23}^2$  fits. Both unknowns are measured with errors much larger than those expected from two-parameters contours. This must be compared with the results of the previous section, where it has been shown that solar parameter uncertainties have a negligible impact.

Consider first the left panel of Fig. 5: the results from a three-parameters fit in  $(\theta_{13}, \delta, \theta_{23})$ . Notice that, being  $\theta_{23}$  a fitting variable in the whole range  $\theta_{23} \in [36^{\circ}, 55^{\circ}]$ , the effect of the "octant ambiguity" is automatically taken into account by the three-parameters  $\chi^2$  function. For this reason the three-parameters contours labelled as "true" and "octant" are identical. Notice also that this is not the case for the two-parameters contours, where the choice of  $s_{oct}$  is reflected in contours located at different values of  $\theta_{13}$  with respect to the input  $\bar{\theta}_{13}$ . For  $\bar{\theta}_{13} = 7^{\circ}$  we can see that a large error in

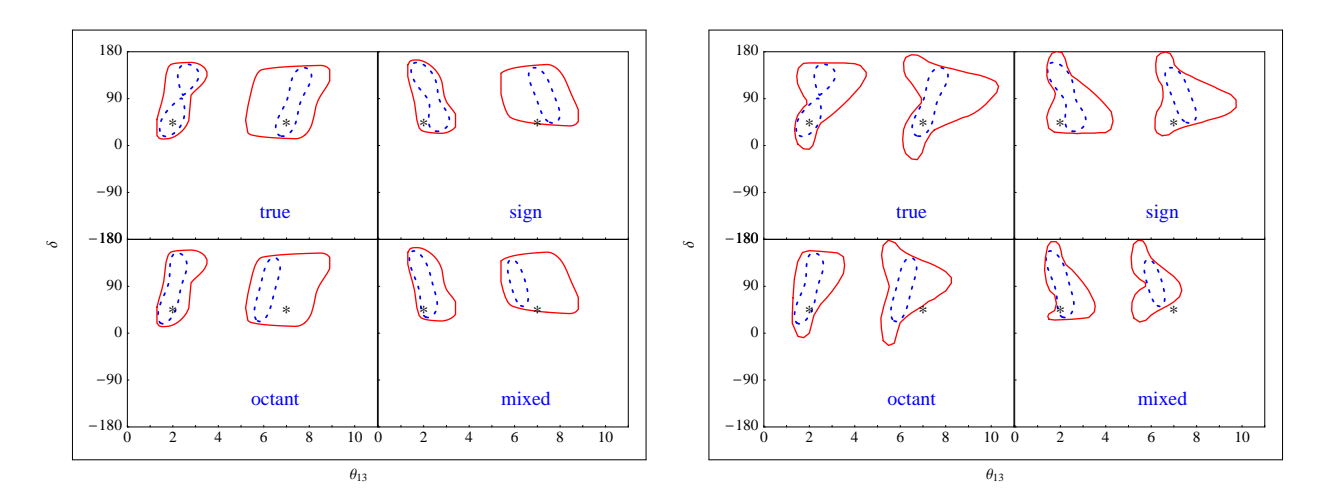


Fig. 5. Comparison of the projection of three-parameters 90% CL contours onto the  $(\theta_{13}, \delta)$  plane (solid lines) with the corresponding two-parameters 90 % CL contours (dashed lines) after a 10 years run at the  $\beta$ -Beam. Different choices of  $s_{atm}$ ,  $s_{oct}$  are plotted separately. The input parameters (represented by a star) are:  $\bar{\theta}_{13} = 2^{\circ}$ ,  $7^{\circ}$ ,  $\bar{\delta} = 45^{\circ}$ . Left panel:  $x = \theta_{23}$ ; right panel:  $x = \Delta m_{23}^2$ .

 $\theta_{13}$  is induced by the uncertainty in  $\theta_{23}$  (with  $\Delta\theta_{13}$  as large as  $4^{\circ}$ ). This is a consequence of the fact that the leading term in the  $\nu_e \to \nu_\mu$  oscillation probability is proportional to the combination  $\sin^2(2\theta_{13})\sin^2\theta_{23}$ : to compensate a change in  $\theta_{23}$ , a change in  $\theta_{13}$  is needed. For smaller values of  $\bar{\theta}_{13}$  this effect is much smaller. The spread in  $\delta$  is, on the other hand, extremely similar in two- and three-parameters contours. This is a consequence of the fact that a  $\delta$ -dependence would be induced in the fit through the subleading term in the oscillation probability, that is proportional to  $\sin(2\theta_{23})$  and thus less sensitive to changes in  $\theta_{23}$  in the almost symmetric interval considered. Notice that three-parameters contours have a box-like shape, with no strong  $\theta_{13} - \delta$  correlation. Finally, the largest values of  $\theta_{13}$  are observed for both choices of  $s_{atm}$  at lower values of  $\theta_{23}$ , whereas the smallest values of  $\theta_{13}$  are reached for larger values of  $\theta_{23}$ .

Consider now the right panel of Fig. 5: the results from a three-parameters fit in  $(\theta_{13}, \delta, \Delta m_{23}^2)$ . In this case to different choices of  $s_{oct}$  correspond different contours  $(\theta_{23})$  is a fixed external input and not a free parameter in the fit). As in the previous case, a large error in  $\theta_{13}$  is induced by the error on the atmospheric parameter, especially for  $\bar{\theta}_{13} = 7^{\circ}$ . The largest value of  $\theta_{13}$  is associated to the smallest value of  $\Delta m_{23}^2$ , in all plots. A characteristic feature of this fit is the significant  $\delta$ -dependence that can be observed in all plots and that was not present in the fits in  $\theta_{23}$ . The three-parameters 90% CL contours have a triangular shape (the error in  $\delta$  reduces for large values of  $\theta_{13}$ ), pointing to a strong  $\theta_{13} - \delta$  correlation. It is important to stress that, when  $\Delta m_{23}^2$  is the free parameter, the overall error in  $\delta$  is significantly larger in the three-than in the two-parameters contours. For both values of  $\bar{\theta}_{13} = 2^{\circ}$ , 7° roughly half of the  $\delta$ -parameter space is covered. This result, considerably worse than what expected from two-parameters fit, can be compared with the CP-coverage expectation (explained in App. A) for this particular input pair, Fig. 11. For both methods, a rather large error

in  $\delta$  is indeed expected.

It is clear from Fig. 5 that both atmospheric parameter uncertainties are extremely important in the measurement of  $\theta_{13}$  and  $\delta$ : the three-parameters 90% CL allowed regions are considerably worse than those obtained with two-parameters fits. In particular, for the shown input pairs,  $\delta$  would remain completely unknown in the interval  $\delta \in [0, \pi]$  and  $\theta_{13}$  would be known only with a large error.

As an example of how the situation can be improved when using reduced uncertainties on the atmospheric parameters, in Fig. 13 we present the projection of the threedimensional 90% CL contours onto the  $(\theta_{13}, \delta)$  plane using the expected uncertainties on the atmospheric parameters after T2K-I (last column of Tab. 1):  $\theta_{23} \in [38^{\circ}, 43^{\circ}]$  –  $[48^{\circ}, 52^{\circ}]$  and  $\Delta m_{23}^2 \in [2.42, 2.61] \times 10^{-3} \text{ eV}^2$  for  $s_{atm} = + \text{ and } \Delta m_{23}^2 \in [2.46, 2.64] \times 10^{-3}$  $eV^2$  for  $s_{atm} = -$ , [42]. The octant-ambiguity (that will not be solved at T2K-I) recover its discrete nature: separate regions of the parameter space will be spanned by different choices of  $s_{oct}$ . In this case, all choices of the two discrete variables  $s_{atm}$  and  $s_{oct}$  are presented together and no comparison with two-parameters contours is shown. In top panels  $x = \theta_{23}$ ; in bottom panels  $x = \Delta m_{23}^2$ . The results of the three-parameters fit with expected uncertainties (right panels), are directly compared with the results presented in Fig. 5 computed with the present uncertainties (left panels). The reduction of the uncertainties on the atmospheric parameters has indeed an important effect on the measurement of  $\theta_{13}$  and  $\delta$ . As it can be seen in the right panels of Fig. 13 a significant reduction of the  $\theta_{13}$ -spread is achieved, with plots resembling those obtained with standard two-parameters contours and fixed external atmospheric parameters (see Refs. [48,27]). The  $\delta$ -spread is also reduced considerably with respect to the results obtained with present uncertainties. These comments apply to both  $\theta_{13}=2^{\circ},7^{\circ}$ . Notice that, as expected being  $\theta_{23}$  restricted to one octant only, the octant- and mixed- ambiguities show themselves as separate contours in the  $(\theta_{13}, \delta)$  plane, as for two-parameters fits.

A final comment on the impact of the uncertainties on the atmospheric parameters on the measurement of  $\theta_{13}$  and  $\delta$  at the low-gamma  $\beta$ -Beam is in order. We have shown that, with present uncertainties, the measurement of the two unknowns in the PMNS mixing matrix is severely spoiled. Errors as large as  $\Delta\theta_{13}\simeq 4^{\circ}$  are found, and half of the parameter space in  $\delta$  is spanned for different values of  $\bar{\delta}$ . This corresponds to a CP-coverage  $\xi\simeq 0.5$ , a value that spoils completely the possibility to distinguish a CP-violating signal from a CP-conserving one at the considered facility (see App. A). A significant reduction in the uncertainties on the atmospheric parameters is mandatory if we plan to use such a facility to look for  $\delta$ . If  $\theta_{23}$  and  $\Delta m_{23}^2$  can be measured at the T2K-I experiment with the expected precision and for any value of  $\bar{\theta}_{23}$ , only then the results of present two-parameters studies [21,27,48,26] for facilities of this kind can be considered reliable.

In App. B we present the results for different choices of  $\bar{\delta}$ , to illustrate the generality of the results above.

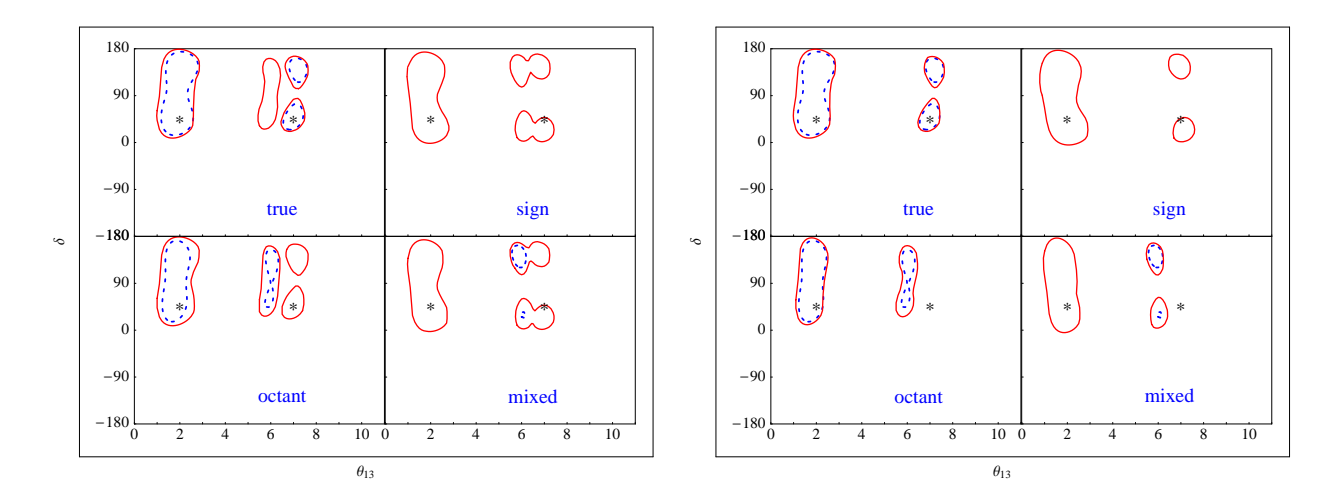


Fig. 6. Comparison of the projection of three-parameters 90% CL contours onto the  $(\theta_{13}, \delta)$  plane (solid lines) with the corresponding two-parameters 90% CL contours (dashed lines) after a 2+8 years run at the Super-Beam. Different choices of  $s_{atm}$ ,  $s_{oct}$  are plotted separately. The input parameters (represented by a star) are:  $\bar{\theta}_{13} = 2^{\circ}$ ,  $7^{\circ}$ ,  $\bar{\delta} = 45^{\circ}$ . Left panel:  $x = \theta_{23}$ ; right panel:  $x = \Delta m_{23}^2$ .

## 6.3 The atmospheric sector at the Super-Beam

We now repeat the analysis of the impact of present and expected uncertainties on the atmospheric sector parameters in the measurement of  $\theta_{13}$  and  $\delta$  at a different facility: the SPL Super-Beam. Again, two distinct three-parameters fits in  $\theta_{13}$ ,  $\delta$  and  $\theta_{23}$  (for fixed  $\Delta m_{23}^2$ ) or  $\Delta m_{23}^2$  (for fixed  $\theta_{23}$ ) have been performed, with the Super-Beam running 2 years with  $\pi^+$  and 8 years with  $\pi^-$  to accumulate comparable statistics for neutrinos and antineutrinos. A significant difference between this facility and the low-gamma  $\beta$ -Beam considered previously is in that the  $\nu_{\mu}$  disappearance channel at the Super-Beam reduces the uncertainties on the atmospheric parameters, as it can be seen in Fig. 3 (whereas the  $\nu_e$  disappearance channel is useless to this purpose, see Ref. [48]). In this case we therefore do not present results using "present" and "expected" uncertainties, but we just combine the results from the appearance and disappearance channel. We have checked that using a "pessimistic" 5% systematic error in the disappearance channel does not change significantly our results.

The comparison between two- and three-parameters fits is presented in Fig. 6. In the left panel we have fixed  $\Delta m^2_{atm} = 2.5 \times 10^{-3} \text{ eV}^2$  and drawn the projection of the three-dimensional contours for  $\chi^2(\theta_{13}, \delta, \theta_{23})$ , for  $\theta_{23} \in [36^\circ, 55^\circ]$  (see Tab. 1). In the right panel we have fixed  $\theta_{23} = 40^\circ$  and drawn the projection of the three-dimensional contours for  $\chi^2(\theta_{13}, \delta, \Delta m^2_{23})$ , for  $\Delta m^2_{23} \in [2.3, 2.9] \times 10^{-3} \text{ eV}^2$  (see Tab. 1 and Sect. 5.2). The input values for the two unknowns are  $\bar{\theta}_{13} = 2^\circ, 7^\circ$  and  $\bar{\delta} = 45^\circ$ .

The main difference between two- and three-parameters contours resides in that in the latter we observe some clones absent in the two-parameters plots. This is a consequence of the not satisfactory expected improvement on the error in  $\theta_{23}$  and  $\Delta m_{23}^2$  for  $\theta_{23} = 40^\circ$ .

Also in this case the measurement of  $\theta_{13}$  and  $\delta$  is severely affected by the uncertainties on the atmospheric parameters. Somewhat smaller errors are found in  $\theta_{13}$  and  $\delta$  with respect to the  $\beta$ -Beam case, but still almost half of the parameter space in  $\delta$  is spanned for different values of  $\bar{\delta}$ . A crucial point is that it does not seem that the  $\nu_{\mu}$  disappearance channel is capable of a significant reduction in the error on the atmospheric mixing angle  $\theta_{23}$ . The T2K-I experiment will therefore be crucial, if indeed the expected precision in  $\theta_{23}$  can be met for any value of  $\bar{\theta}_{23}$ .

In App. B we present the results for different choices of  $\bar{\delta}$ , to illustrate the generality of the results above.

## 6.4 The atmospheric sector at the Neutrino Factory

We repeat the analysis of the impact of atmospheric parameters uncertainties in the measurement of  $\theta_{13}$  and  $\delta$  at a third facility: the CERN-based SPL-fuelled 50 GeV Neutrino Factory. We want to show in this way how the results of Sects. 6.2 and 6.3 are quite general and must be taken into account at any facility that is considered when looking for  $\theta_{13}$  and  $\delta$ .

As before, two distinct three-parameters fit in  $\theta_{13}$ ,  $\delta$  and  $\theta_{23}$  (for fixed  $\Delta m_{23}^2$ ) or  $\Delta m_{23}^2$  (for fixed  $\theta_{23}$ ) have been performed, with the Neutrino Factory running 5 years with  $\mu^+$  and 5 years with  $\mu^-$ .

In the absence of an updated analysis of the expected reduction of atmospheric parameters uncertainties at this facility through  $\nu_{\mu} \rightarrow \nu_{\mu}$ ,  $\nu_{e} \rightarrow \nu_{e}$  and  $\nu_{\mu} \rightarrow \nu_{\tau}$  (see Ref. [43,44] for old analyses), we only present results combining the two appearance channels  $\nu_{e} \rightarrow \nu_{\mu}$  (i.e. the "golden" channel) and  $\nu_{e} \rightarrow \nu_{\tau}$  (i.e. the "silver" channel) for both polarities. We use the expected uncertainties after T2K-I, in order to get a preliminar understanding of the impact of atmospheric parameter uncertainties at this facility.

The comparison between two- and three-parameters fits is presented in Fig. 7. In the left panel we have fixed  $\Delta m^2_{atm} = 2.5 \times 10^{-3} \; \mathrm{eV^2}$  and drawn the projection of the three-dimensional contours for  $\chi^2(\theta_{13}, \delta, \theta_{23})$ , for  $\theta_{23} \in [38^\circ, 43^\circ] - [48^\circ, 52^\circ]$  (see Tab. 1). In the right panel we have fixed  $\theta_{23} = 40^\circ$  and drawn the projection of the three-dimensional contours for  $\chi^2(\theta_{13}, \delta, \Delta m^2_{23})$ , for  $\Delta m^2_{23} \in [2.4, 2.7] \times 10^{-3} \; \mathrm{eV^2}$  (see Tab. 1 and Sect. 5.2). The input values for the two unknowns are  $\bar{\theta}_{13} = 2^\circ, 7^\circ$  and  $\bar{\delta} = 42^\circ$ .

First of all notice that at the Neutrino Factory the sign and mixed degeneracies are solved, being the magnetized iron detector with a L=3000 km baseline extremely sensitive to matter effects and thus capable to measure  $s_{atm}$ . For this reason we only present two panels, corresponding to two possible choices of the  $\theta_{23}$ -octant,  $s_{oct}=\pm \bar{s}_{oct}$ . As for the SPL Super-Beam, for small  $\bar{\theta}_{13}$  the two- and three-parameters contours practically coincide. On the other hand, for  $\bar{\theta}_{13}$  large we must make a distinction between  $s_{oct}=\bar{s}_{oct}$  and  $s_{oct}=-\bar{s}_{oct}$ : whereas the impact of the atmospheric uncertainties for  $s_{oct}=\bar{s}_{oct}$  is marginal (something already observed in [9], where the covariance matrix

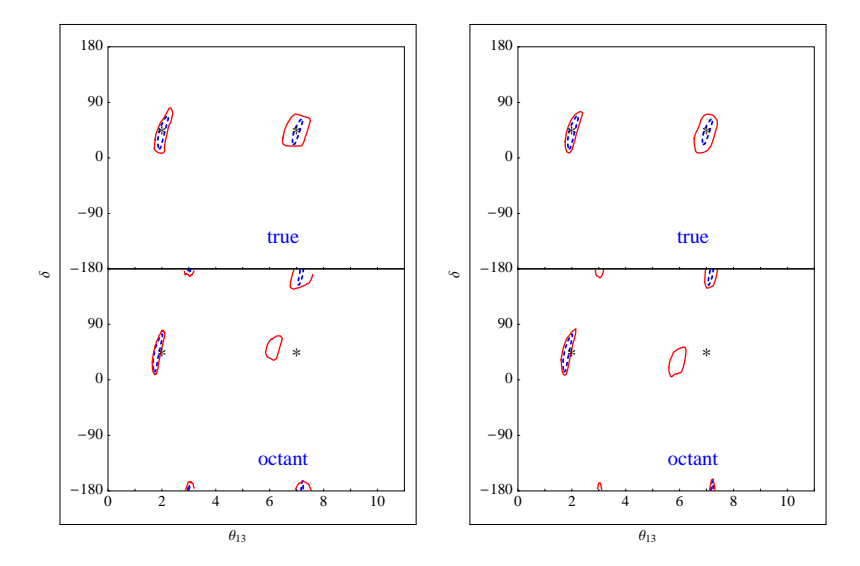


Fig. 7. Comparison of the projection of three-parameters 90% CL contours onto the  $(\theta_{13}, \delta)$  plane (solid lines) with the corresponding two-parameters 90 % CL contours (dashed lines) after a 5+5 years run at the Neutrino Factory. Different choices of  $s_{oct}$  are plotted separately. The input parameters (represented by a star) are:  $\bar{\theta}_{13} = 2^{\circ}, 7^{\circ}, \bar{\delta} = 42^{\circ}$ . Left panel:  $x = \theta_{23}$ ; right panel:  $x = \Delta m_{23}^2$ .

approach was adopted and only the right choice of the  $\theta_{23}$ -octant was considered), we notice how extra octant clones are present in the three-parameters contours that are absent in the two-parameters ones when the wrong choice of  $s_{oct}$  is taken. This happens because in the three-dimensional parameter space  $\theta_{23}$  cooperates with  $\theta_{13}$  to identify a low  $\chi^2$  region with  $\delta \simeq \bar{\delta}$  but with  $\theta_{13} < \bar{\theta}_{13}$ .

As for the other facilities, we have seen that the impact of the uncertainties on the atmospheric parameters on the measurement of  $\theta_{13}$  and  $\delta$  at the Neutrino Factory is relevant (albeit perhaps not as important as for the  $\beta$ -Beam and the Super-Beam previously discussed). Again, we stress that the loss in precision is more important for large  $\bar{\theta}_{13}$  than for small  $\bar{\theta}_{13}$ , a region of the PMNS parameter space that will be selected or excluded by the approaching T2K-I experiment. This is indeed a crucial problem for precision measurements of the PMNS matrix elements.

In App. B we present the results for different choices of  $\bar{\delta}$ , to illustrate the generality of the results above.

## 7 CP-violation discovery potential

Eventually, in Figs. 8-10 we compare the sensitivity to  $(\theta_{13}, \delta)$  obtained with a two-parameters fit in  $(\theta_{13}, \delta)$  or a three-parameters fit in  $(\theta_{13}, \delta, \theta_{23})$  or  $(\theta_{13}, \delta, \Delta m_{23}^2)$  at the three considered facilities. The  $3\sigma$  contours have been computed as in Ref. [48]: at a fixed  $\bar{\theta}_{13}$ , we look for the smallest (largest) value of  $|\bar{\delta}|$  for which the two- (three-)

parameters  $3\sigma$  contours of any of the degenerate solutions (true, sign, octant and mixed) do not touch  $\delta = 0^{\circ}$  nor  $\delta = 180^{\circ}$ . Notice that, although the input  $\bar{\theta}_{13}$  value is fixed, the clones can touch  $\delta = 0^{\circ}$ ,  $180^{\circ}$  at  $\theta_{13} \neq \bar{\theta}_{13}$ , also<sup>5</sup>. The outcome of this procedure is finally plotted, representing the region in the  $(\theta_{13}, \delta)$  parameter space for which a CP-violating signal is observed at  $3\sigma$ . Within this approach we can thus take fully into account the impact of the parameter degeneracies in the CP-violation discovery potential of the three facilities. As for the previous section, we have applied a 2% systematic error on disappearance channels and a 5% systematic error on appearance channels. As in the previous section we used the expected errors on the atmospheric parameters after T2K-I for the three-parameters fits at the  $\beta$ -Beam and the Neutrino Factory. The SPL Super-Beam analysis relies on SPL data, only (see Sect. 5.2).

Notice that results are given for the whole allowed range in  $\delta$ ,  $\delta \in [-180^{\circ}, 180^{\circ}]$ . This is particularly appropriate, since only an approximate symmetry is observed for  $|\delta| \geq \pi/2$  and  $|\delta| \leq \pi/2$  and no symmetry at all between positive and negative  $\delta$  in the case of the  $\beta$ -Beam and of the Neutrino Factory.

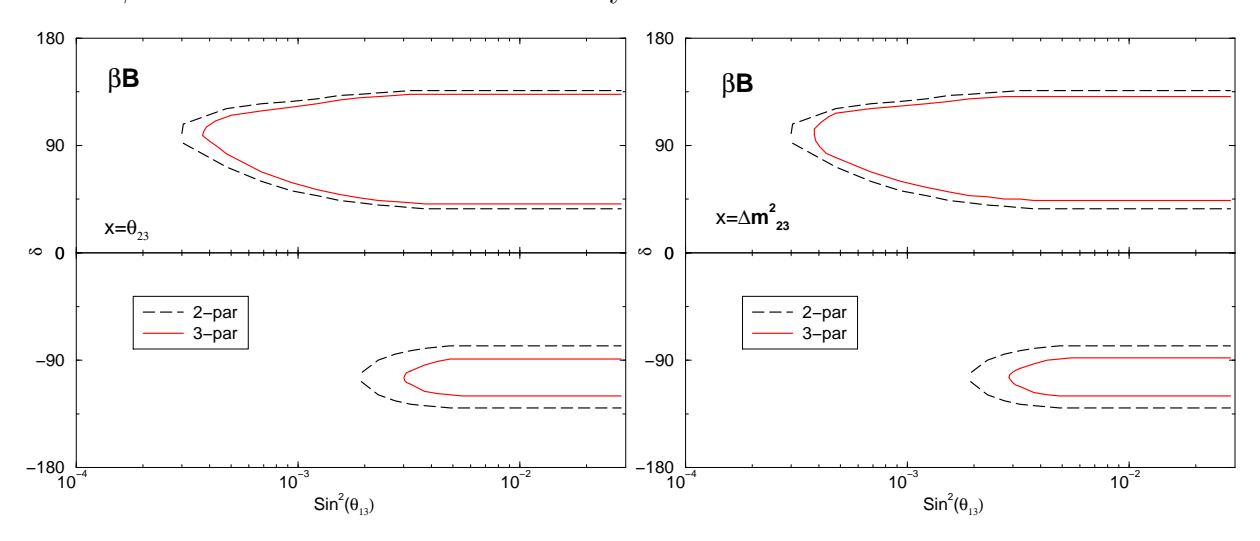


Fig. 8. CP-violation discovery potential after 10 years at the low- $\gamma$   $\beta$ -Beam.

Consider first Fig. 8, that refers to  $\beta$ -Beam results. Notice that the discovery potential is not symmetric for positive and negative values of  $\delta$ , as it has already been observed in Ref. [48]. This asymmetric behaviour of the  $\beta$ -Beam is indeed a statistical mirage caused by the low background in the appearance antineutrino sample and the high background in the appearance neutrino one (see Ref. [27]). A proper statistical treatment should be performed, following Ref. [52], to get rid of this asymmetry for small  $\sin^2 \theta_{13}$ : the treatment, however, is extremely time-consuming and we do not consider meaningful applying it here. A further asymmetry can be observed in the different behaviour of the

<sup>&</sup>lt;sup>5</sup> This is not the case of Fig. 11 in Ref. [27], where the excluded region in  $\delta$  at fixed  $\bar{\theta}_{13}$  in the absence of a CP-violating signal at 90% CL is presented. In practice, in that figure we compare  $N_{\pm}(\bar{\theta}_{13}, \delta)$  with  $N_{\pm}(\bar{\theta}_{13}, 0^{\circ})$ , thus obtaining a one-parameter sensitivity plot in  $\delta$  only.

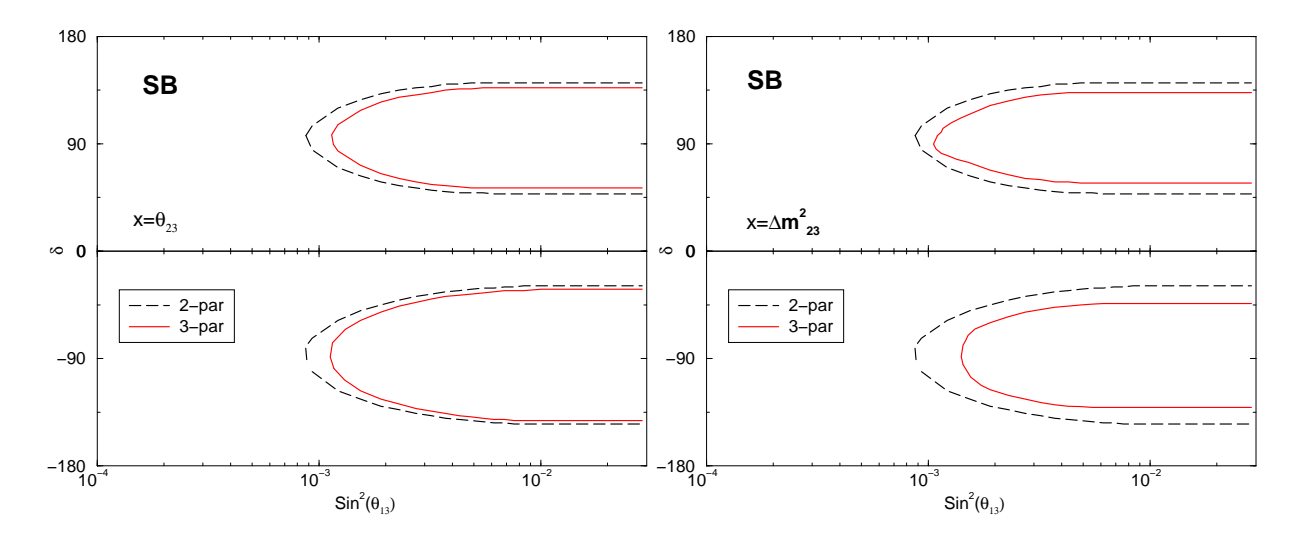


Fig. 9. CP-violation discovery potential after 2+8 years at the SPL Super-Beam.

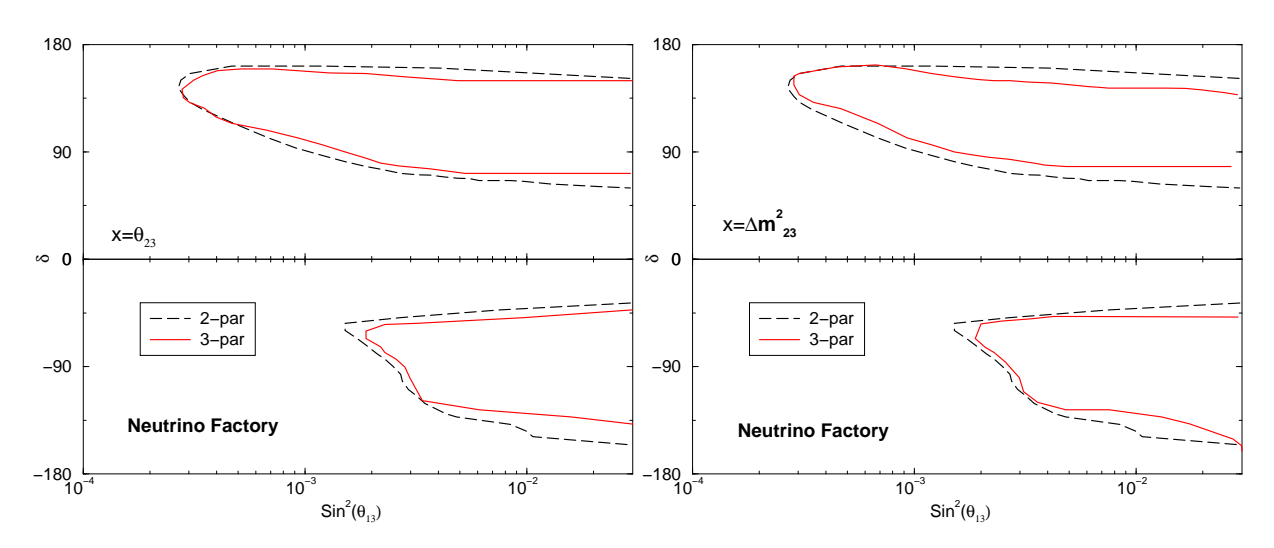


Fig. 10. CP-violation discovery potential after 5+5 years at the 50 GeV Neutrino Factory.

three-parameters  $3\sigma$  contours projection onto the  $(\theta_{13}, \delta)$  plane for positive and negative values of  $\delta$ : whereas for  $\delta > 0$  we observe that the smallest value of  $\sin^2\theta_{13}$  for which a CP-violating phase can be distinguished from a null result goes from  $[\sin^2\theta_{13}]_{min} = 3 \times 10^{-4} \to 5 \times 10^{-4}$ , for  $\delta < 0$  we get  $[\sin^2\theta_{13}]_{min} = 2 \times 10^{-3} \to 4 \times 10^{-3}$  for both the  $\theta_{23}$  and  $|\Delta m_{23}^2|$  fits. A small loss in the discovery potential of this facility with respect to the two-parameters fit is observed in both three-parameters fits for negative  $\delta$ . In particular, the region in which a CP-violating signal can be distinguished from a CP-conserving one goes from  $\delta \in [-80^{\circ}, -130^{\circ}] \to \delta \in [-90^{\circ}, -120^{\circ}]$ .

Consider now Fig. 9, that refers to Super-Beam results. The strong asymmetry for positive and negative  $\delta$  is not observed in this case, both for two- and three-parameters fits. The impact of the third fitting variable, being it  $\theta_{23}$  or  $\Delta m_{23}^2$ , is a rather small loss in the minimum value of  $\sin^2 \theta_{13}$  for which a CP-violating phase is distinguished

from a null result:  $[\sin^2\theta_{13}]_{min} = 9 \times 10^{-4} \rightarrow 1.2 \times 10^{-3}$  for  $x = \theta_{23}$  and  $[\sin^2\theta_{13}]_{min} = 9 \times 10^{-4} \rightarrow 1.4 \times 10^{-3}$  for  $x = \Delta m_{23}^2$ . The loss in the  $\delta$ -interval that is distinguishable from a null result is rather small for three-parameters fits in  $\Delta m_{23}^2$  and negligible when fitting in  $\theta_{23}$ .

For the Neutrino Factory, Fig. 10, we observe a mixed situation: a strong asymmetry between positive and negative  $\delta$  regions (as for the  $\beta$ -Beam), but a very small difference between two- and three-parameters fits (as for the Super-Beam). The asymmetry, however, it is not a consequence of asymmetric signal-to-noise ratios <sup>6</sup> as for the  $\beta$ -Beam but, rather, of a "parametric conspiracy" that for the chosen values of energy and baseline results in clones that for many negative values of  $\bar{\delta}$  move toward  $\delta = 0^{\circ}$  or  $\delta = 180^{\circ}$  [47], thus preventing a clean identification of a CP-violating signal (see Figs. 22-26). The impact of the third fitting variable, being it  $\theta_{23}$  or  $\Delta m_{23}^2$ , is a rather small loss in the minimum value of  $\sin^2 \theta_{13}$  for which a CP-violating phase is distinguished from a null result for negative  $\bar{\delta}$ :  $[\sin^2 \theta_{13}]_{min} = 1.5 \times 10^{-3} \rightarrow 2 \times 10^{-3}$ . On the other hand, for positive values of  $\bar{\delta}$ ,  $[\sin^2 \theta_{13}]_{min} = 2.5 \times 10^{-4}$  both for two- and three-parameters fits.

#### 8 Conclusions

The simultaneous measurement of  $\theta_{13}$  and  $\delta$  has been often performed in the literature considering the solar and atmospheric PMNS parameters as external quantities fixed to their best fit values. This is an approximation that has been adopted to get a first insight on the problems related to the  $(\theta_{13}, \delta)$  measurement. The experimental uncertainties on these parameters can in principle affect the measurement of the unknowns, and it seemed important to us to perform an analysis that could go beyond the two-parameters fits presented in the literature.

In this paper we therefore have tried to study the impact that solar and atmospheric sector parameter uncertainties have on the measurement of  $\theta_{13}$  and  $\delta$  at three out of the many proposed setups, the standard low- $\gamma$   $\beta$ -Beam, the 4 MWatt SPL Super-Beam and the 50 GeV SPL-fuelled Neutrino Factory. By doing this we wanted to catch the characteristic features of the inclusion of external parameters uncertainties in a  $(\theta_{13}, \delta)$  measurement.

Our first goal has been to identify which of the external parameters affects the most the results of two-parameters fits. To do so we have performed a series of three-parameters fits in  $\theta_{13}$ ,  $\delta$  and one of the other parameters ( $\theta_{12}$ ,  $\Delta m_{sol}^2$ ,  $\theta_{23}$  and  $\Delta m_{atm}^2$ ) in turn as the third fitting variable and compared our results with standard two-parameters fits. It turned out that the impact of solar parameters uncertainties on the measurement of ( $\theta_{13}$ ,  $\delta$ ) is negligible, in practice, whereas present uncertainties on the atmospheric

<sup>&</sup>lt;sup>6</sup> It must also be reminded that for 5 years of data taking in each polarity, a smaller statistics is accumulated in the wrong-sign muon sample for initial  $\mu^-$  than for initial  $\mu^+$ , due to the different  $\nu N$  and  $\bar{\nu} N$  cross-sections. This reduces the sensitivity to  $\theta_{13}$  for negative  $\bar{\delta}$ .

parameters are large enough to modify in a significant way the results of two-parameters fits. In particular, we have noticed that the main cause of the worsening from two-to three-parameters fits are the wide displacements of the so-called *clones*, parametric degeneracies due to multiple solutions of eqs. (3)-(6), as a consequence of small changes in the external parameters. These results are general to all the considered facilities.

We have then focused our attention on how the reduction of the atmospheric parameters uncertainties could ameliorate the previous results. To this respect, the three facilities we have considered are on different footing. On one side, the  $\nu_e$  disappearance channel at the standard low- $\gamma \beta$ -Beam cannot improve on its own the present measurement of the atmospheric parameters. This facility, therefore, must rely on other experiments to meet its goal on  $\theta_{13}$  and  $\delta$ . Luckily enough, it turns out that the precision on  $\theta_{23}$  and  $\Delta m_{23}^2$  expected at the approved T2K-phase I experiment, if met, would be enough to improve our three-parameters fits and reproduce the results of two-parameters fits in the literature (that, however, were not so good). On the other hand, we have shown that the  $\nu_{\mu}$  disappearance channel at the 4 MWatt SPL Super-Beam does improve the present errors on the atmospheric parameters. This facility, therefore, should not necessarily rely on external inputs. The combination of appearance and disappearance data, indeed, improve significantly our three-parameters fits. However,  $\theta_{23}$  is not measured well enough and extra clones are still present in the  $(\theta_{13}, \delta)$  that are absent in two-parameters contours. Finally, the Neutrino Factory has certainly the potential to improve significantly the precision on the atmospheric parameters through  $\nu_e$  and  $\nu_\mu$ disappearance and the  $\nu_{\mu} \rightarrow \nu_{\tau}$  appearance channel, something that we have not studied in this paper. Using the errors on  $\theta_{23}$  and  $\Delta m_{23}^2$  expected at the T2K-I experiment we have checked that extra clones are present in three-parameters fits that were absent in the two-parameters analysis. This is a clear indication of the fact that the problem we are addressing is common to all the facilities, not only to the low- $\gamma \beta$ -Beam or the SPL Super-Beam. It is not sufficient to just wait and see, but it must be taken into account when envisaging future facilities to look for  $\theta_{13}$  and  $\delta$ .

To include the impact of external parameters uncertainties, other methods than direct multi-parameter fits have been proposed in the literature. For this reason, we have presented a direct comparison of our three-parameters fit results with the so-called CP-coverage introduced in Ref. [18]. We have shown that in both methods a significant worsening of two-parameters fits arise as a consequence of the inclusion of errors on the external parameters in the fit. Whereas the CP-coverage method, however, can be quite useful to condense informations about the CP-sensitivity of a facility irrespectively of the specific input pair  $(\bar{\theta}_{13}, \bar{\delta})$  considered, direct three-parameters fits offer a detailed information for both  $\theta_{13}$  and  $\delta$  for specific points in the parameter space. We believe that the two methods are, in some sense, complementary and should be combined to get a thorough view of the performance of a specific facility designed to measure the  $(\theta_{13}, \delta)$  pair. To this scope we have presented in App. B the results of a series of three-parameters fits for the standard low- $\gamma$   $\beta$ -Beam, the 4 MWatt SPL Super-Beam and the 50 GeV Neutrino Factory for different choices of the input parameters.

Eventually, we have studied the impact of the atmospheric parameters uncertainties in the CP-violation discovery potential of the three considered facilities. Our results show that the discovery potential at the standard low- $\gamma$   $\beta$ -Beam and at the SPL Super-Beam is somewhat reduced for negative values of  $\delta$  when uncertainties on  $\theta_{23}$  and  $\Delta m_{23}^2$  are taken into account. On the other hand the Neutrino Factory appears less affected by the inclusion of external parameter errors.

In conclusion, we think that this paper shows that present uncertainties on atmospheric parameters are indeed too large so that the widely adopted approximation of fixing  $\theta_{23}$  and  $\Delta m_{23}^2$  to their present best fit values be reliable. A new phase of experiments that could improve these uncertainties are needed. The precision that is expected on the atmospheric parameters at the T2K-I experiment is shown to be such that three-parameters fits could reproduce the results of two-parameters fits presented in the literature. This experiment is therefore a crucial step in the way to the measurement of the two PMNS unknowns, if the precision goals can indeed be met.

The same kind of analysis we presented here must be clearly repeated at all of the proposed setups, something that goes beyond the scope of this paper but is extremely important to establish on solid grounds the quest for  $\theta_{13}$  and leptonic CP violation in the near future.

## Acknowledgements

We would like to thank E. Fernández-Martínez for extremely useful discussions and comments, D. Autiero, Y. Declais, B. Gavela, J.J. Gomez-Cadenas, P. Hernandez, P. Lipari, E. Lisi, M. Lusignoli, O. Mena and P. Migliozzi for discussions. A.D. and S.R. acknowledge the M.C.Y.T. *Ramón y Cajal* program and the BENE european network for financial support.

## Appendix A

In this Appendix we review some of the statistical methods that have been proposed in the literature to take into account uncertainties on the external parameters in the measurement of  $(\theta_{13}, \delta)$ .

## 1) Comparison between naive two- and three-parameters fit

The obvious difference is in the CL contours that can be drawn in the two cases: for two-parameters fit the 90% CL corresponds to  $\Delta\chi^2=4.61$ , whereas for three-parameters fit is  $\Delta\chi^2=6.25$ . As a consequence, when a single minimum is found the projection of a three-parameters fit onto the two-dimensional contour is, in general, a bit larger. The second, not obvious, difference resides in that in the three-parameters fit the three-dimensional manifold automatically allows for a displacement of the clones solutions arranging for a lower  $\chi^2$  at the relative minima. This is indeed the case for

the clones corresponding to wrong choices of  $s_{atm}$  and of the  $\theta_{23}$ -octant (see [47], also). If the clones location moves in the three-dimensional manifold, the resulting projection onto the plane can be much larger than the two-parameters contour. This is indeed the main result of this paper and is discussed at length in Sect. 6.

## 2) Inclusion of a covariance matrix in the two-parameters fit

A fixed error range for any non-fitted parameter can be taken into account introducing a covariance matrix in the  $\chi^2$  function as follows:

$$\chi_{\{\bar{\alpha}\}}^{2}(\theta_{13}, \delta) = \sum_{i,j} \left\{ \left[ N_{i}(\theta_{13}, \delta) - N_{i}(\bar{\theta}_{13}, \bar{\delta}) \right] C_{ij}^{-1} \left[ N_{j}(\theta_{13}, \delta) - N_{j}(\bar{\theta}_{13}, \bar{\delta}) \right] \right\}_{\{\bar{\alpha}\}}$$
(12)

where  $C_{ij}$  is the covariance matrix, i, j refer to different channels at the same experiment or to different experiments and  $\{\bar{\alpha}\}$  is a given set of external parameters. If the errors on the entries i and j of the covariance matrix are statistically independent, C is

$$C_{ij} = \delta_{ij} \, \delta N_i^2 + \sum_{\alpha=1}^{N_{\alpha}} \frac{\partial N_i}{\partial \alpha} \frac{\partial N_j}{\partial \alpha} \sigma^2(\alpha) \tag{13}$$

where  $\sigma(\alpha)$  is the  $1\sigma$  error on the parameter  $\alpha$ . This procedure, followed in [9] for the Neutrino Factory and in [21] for the facilities considered in this paper, reproduces the enlargement of the two-parameters CL contours observed from a multi-parameter fit projected onto the  $(\theta_{13}, \delta)$  plane. However, within this approach, the clones locations are not free to move in the multi-dimensional manifold to arrange for a lower  $\chi^2$ : they are indeed stucked to the location in the  $(\theta_{13}, \delta)$  plane that can be computed once known the external (fixed) parameters (see [47], again, and [53], Sect. 3.3). The displacement of the relative minima is indeed the characteristic feature of the multi-parameter fit, where  $N_{\alpha}$  external parameters cooperate with  $\theta_{13}$  and  $\delta$  to locate lower  $\chi^2$  regions than those found in a two-parameters fit with fixed external parameters. The resulting regions are therefore large than those obtained including the covariance matrix in a two-parameters fit.

# 3) CP-coverage and marginalization over $N_{\alpha}$ external parameters

A parameter that can be used to compare in a condensed way the capability of different setups to measure the CP-violating phase  $\delta$  has been proposed in [18]. The CP-coverage is defined as follows:

$$\xi(\bar{\delta}) = \text{Coverage in } \delta = \frac{1}{2\pi} U_{I=1}^{N_{deg}} \Delta_I(\bar{\delta}),$$
 (14)

is the fraction of the  $\delta$ -parameter space (i.e.,  $2\pi$ ) that is allowed at a given CL as a result of a measure when the input parameter is  $\bar{\delta}$ . The sum goes over  $N_{deg}$  possible allowed regions induced by parameter degeneracies, each of them spanning an interval  $\Delta_I(\bar{\delta})$  of the parameter space. We take the union of these intervals to take into account

possible partial overlaps of the  $\Delta_I(\bar{\delta})$ . The smaller the CP-coverage, the better the measurement of  $\delta$  at a given experiment. In particular, to distinguish a maximally CP-violating signal (i.e.,  $\bar{\delta} = \pm 90^{\circ}$ ) at a given experiment from  $\delta = 0^{\circ}$  or  $\delta = 180^{\circ}$ , the CP-coverage must be less than 0.5.

The definition of the CP-coverage above is, however, incomplete: we must still define how the  $\Delta_I(\bar{\delta})$  intervals are computed and which is the dependence of  $\xi(\bar{\delta})$  on other parameters. Indeed, if all the parameters of the PMNS matrix but  $\delta$  were measured,  $\xi(\bar{\delta})$  would be just an involute way to express the expected error of an experiment for a certain value of  $\bar{\delta}$ . This has been called the "CP-pattern", see Fig. 4(right) in Ref. [53]. If, on the other hand,  $\theta_{13}$  is also an unknown parameter, we can think of defining a function  $\xi(\bar{\theta}_{13}, \bar{\delta})$  and to plot it as a function of different values of  $\bar{\theta}_{13}$  (called "CP-scaling" in Ref. [53]) for a fixed value of  $\bar{\delta}$ . In this second case, for the particular value  $\bar{\delta} = 0^{\circ}$ , the "CP-scaling" as a function of  $\bar{\theta}_{13}$  is nothing else that the CP-sensitivity. For example, Fig. 5 in Ref. [21] or Fig. 11 of Ref. [27] represent the sensitivity to  $\delta$  for varying  $\bar{\theta}_{13}$  defined as a one-parameter fit where all mixing parameters have been measured but  $\delta$  and  $\theta_{13}$ . The same idea is presented in Fig. 6 of Ref. [21] and Fig. 13 of Ref. [26], where the plot represents the capability to distinguish a non-vanishing  $\delta$  from  $\delta = 0^{\circ}$  or  $\delta = 180^{\circ}$  at a given one-parameter CL  $^{7}$ .

To take into account the fact that, in general, the parameters of the mixing matrix are known only with a finite precision and that  $\theta_{13}$  is completely unknown at present (and thus a one-parameter  $\delta$ -sensitivity plot is generally overestimating the performance of a given experiment), the authors of Ref. [18] have proposed to compute the CP-coverage  $\xi(\bar{\delta})$  by first minimizing a  $(N_{\alpha}+2)$ -parameter  $\chi^2$  over  $N_{\alpha}$  external parameters. In this way, for any input pair  $\bar{\theta}_{13}$  and  $\bar{\delta}$ , a two-dimensional surface of the  $\chi^2$  minimum as a function of  $\theta_{13}$  and  $\delta$  is generated. If we then minimize the resulting function in  $\theta_{13}$ , also, we can deduce a one-dimensional function of  $\delta$  and of the input parameters representing the minimum value of the  $(N_{\alpha}+2)$ -dimensional  $\chi^2$  for a given value of  $\bar{\delta}$ . From this marginalized  $\chi^2$  we can finally compute the allowed  $\Delta_I(\bar{\delta})$  intervals imposing that  $\chi^2_{min}(\delta,\bar{\delta})$  be equal to a given one-parameter CL.

Clearly, this procedure can fail when multiple minima are present at each marginalization step. When multiple minima are present, the minimization procedure will generally look for the absolute minimum. In this way, the information on other relative minima in the  $\chi^2$  can be lost. This is particularly problematic since we know that, due to parametric degeneracies, multiple minima should be present. Marginalization near a second minimum will give a second function  $\chi^2_{min}(\delta,\bar{\delta})$ , from which a new set of  $\Delta_I(\bar{\delta})$  intervals can be found. The procedure suggested in [53] is indeed to marginalize

 $<sup>\</sup>overline{\phantom{a}}$  It should be stressed that it is not completely correct to present this "CP discovery potential" with one-parameter CL contours: being  $\theta_{13}$  a parameter to be fitted together with  $\delta$ , we should consider two-parameters CL contours, instead. In this case the CP discovery potential can be smaller than when only  $\delta$  is left as a free parameter, as a result of the fact that the two-parameters  $\chi^2(\theta_{13}, \delta)$  can be lower than  $\chi^2(\bar{\theta}_{13}, \delta)$  for specific values of  $\theta_{13} \neq \bar{\theta}_{13}$ . This is indeed what reported in Fig. 7 of Ref. [48].

around each of the expected minima in the multi-dimensional  $\chi^2$  and to draw several distinct one-dimensional functions  $\chi^2_{min}(\delta,\bar{\delta})$ . Imposing on any of them the constraint  $\chi^2_{min}(\delta,\delta) = CL$ , the full set of allowed regions in  $\delta$  at a given one-parameter CL for a fixed input  $\bar{\delta}$  is deduced and the  $\xi(\bar{\delta})$  can be finally computed. Since the minimization procedure must be repeated several times (once per expected minima), it is useful to choose the starting point of the minimization algorithm in a clever way. In [53] it is suggested to solve eqs. (3)-(6) as it has been done in Ref. [47] to find the expected clone locations and to use the latter as starting points for the minimization. Applying the previous algorithm it is possible to deduce a  $\xi(\bar{\delta}, \bar{\theta}_{13})$  parameter that reduce significantly the overestimation of the experiment performances in the measurement of  $\delta$  that is typical of the one-parameter  $\delta$ -sensitivity plots. We should therefore compare this procedure with the projection onto the  $\delta$ -axis of our three-parameters fits to understand if a residual overestimation is still present. To this purpose, in Fig. 11 we present the CP-coverage  $\xi(\theta_{13}, \delta)$  and the projection onto the  $\delta$ -axis of the three-parameters CL contours for different values of  $\bar{\theta}_{13}$  and  $\bar{\delta}$ . The results in the figure have been obtained using the considered  $\beta$ -Beam facility, for definiteness.

As it can be seen in the figure, some underestimation of the error on  $\delta$  at the considered experiment is still present when computing  $\xi(\bar{\delta})$  and comparing it with the  $\delta$ -axis projection of the three-parameters fits. The main interest of the CP-coverage parameter is that the algorithm described above can be iterated for any value of  $\bar{\theta}_{13}$  to obtain a "CP-scaling" for any given value of  $\bar{\delta}$ , thus replacing the (poorly reliable) one-parameter  $\delta$ -sensitivity plots. This will give the general picture of the expected error on  $\bar{\delta}$  at a given facility, to be complemented in our opinion with multi-parameter fits to particular values of  $\theta_{13}$  and  $\delta$  to get a robust estimate of the facility performance.

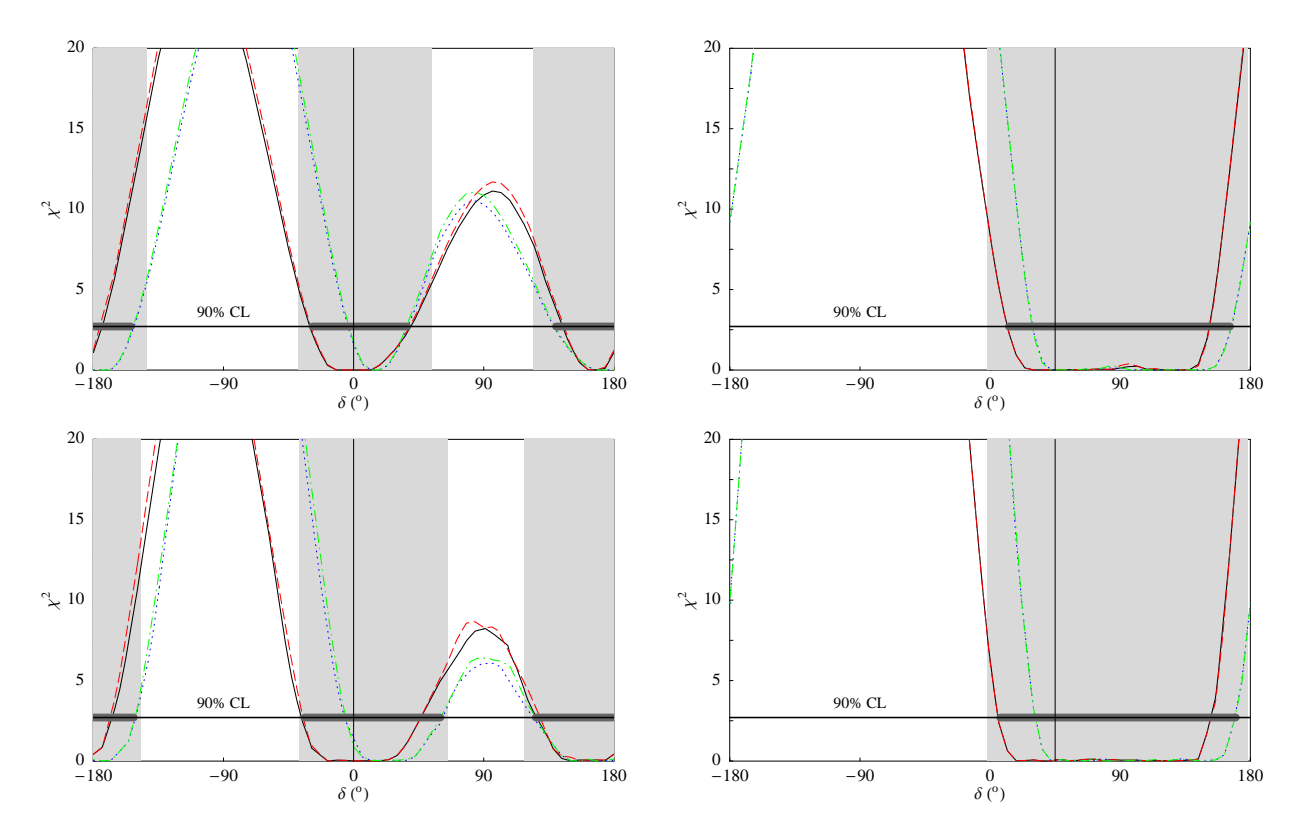


Fig. 11. Comparison of the CP-coverage  $\xi$  and the  $\delta$ -axis projection of the three-parameters 90% CL contour to the same input parameters at the  $\beta$ -Beam. The marginalized  $\chi^2_{min}(\delta,\bar{\delta})$  function is plotted for different choices of  $s_{atm}$  and  $s_{oct}$ :  $s_{atm} = \bar{s}_{atm}, s_{oct} = \bar{s}_{oct}$  (solid);  $s_{atm} = -\bar{s}_{atm}, s_{oct} = \bar{s}_{oct}$  (dotted);  $s_{atm} = \bar{s}_{atm}, s_{oct} = -\bar{s}_{oct}$  (dashed);  $s_{atm} = -\bar{s}_{atm}, s_{oct} = -\bar{s}_{oct}$  (dot-dashed). Horizontal thick black lines are the  $\Delta_I(\bar{\delta})$  intervals and the gray-shaded region are the corresponding three-parameters 90% CL contours. Of the two possible three-parameters fit (i.e., in  $\theta_{23}$  or  $\Delta m^2_{23}$ ), that with the largest error in  $\delta$  is reported. The thin vertical line displays the value of  $\bar{\delta}$  for each plot. The different plots refer to:  $\bar{\theta}_{13} = 2^{\circ}$ ,  $\bar{\delta} = 0^{\circ}$  (top left);  $\bar{\theta}_{13} = 2^{\circ}$ ,  $\bar{\delta} = 45^{\circ}$  (top right);  $\bar{\theta}_{13} = 7^{\circ}$ ,  $\bar{\delta} = 0^{\circ}$  (bottom left);  $\bar{\theta}_{13} = 7^{\circ}$ ,  $\bar{\delta} = 45^{\circ}$  (bottom right). The atmospheric input parameters are  $\bar{\theta}_{23} = 40^{\circ}$ ,  $\Delta m^2_{atm} = 2.5 \times 10^{-3}$  eV<sup>2</sup>.

## References

[1] Y. Fukuda et al. [Super-Kamiokande Collaboration], Phys. Rev. Lett. 81 (1998) 1562 [arXiv:hep-ex/9807003]; M. Ambrosio et al. [MACRO Collaboration], Phys. Lett. B 517 (2001) 59 [arXiv:hep-ex/0106049]; M. H. Ahn et al. [K2K Collaboration], Phys. Rev. Lett. 90 (2003) 041801 [arXiv:hep-ex/0212007]; B. T. Cleveland et al., Astrophys. J. 496 (1998) 505; J. N. Abdurashitov et al. [SAGE Collaboration], Phys. Rev. C 60 (1999) 055801 [arXiv:astro-ph/9907113]; W. Hampel et al. [GALLEX Collaboration], Phys. Lett. B 447 (1999) 127; S. Fukuda et al. [Super-Kamiokande Collaboration], Phys. Rev. Lett. 86 (2001) 5651 [arXiv:hep-ex/0103032]; Q. R. Ahmad et al. [SNO Collaboration], Phys. Rev. Lett. 87 (2001) 071301 [arXiv:nucl-ex/0106015]; K. Eguchi et al. [KamLAND Collaboration], Phys. Rev. Lett. 90 (2003) 021802 [arXiv:hep-ex/0212021].

- [2] C. Athanassopoulos *et al.* [LSND Collaboration], Phys. Rev. Lett. **81** (1998) 1774
   [arXiv:nucl-ex/9709006]; A. Aguilar *et al.* [LSND Collaboration], Phys. Rev. D **64** (2001) 112007 [arXiv:hep-ex/0104049].
- [3] I. Stancu et al. [MiniBooNE collaboration], FERMILAB-TM-2207.
- [4] B. Pontecorvo, Sov. Phys. JETP 6 (1957) 429 [Zh. Eksp. Teor. Fiz. 33 (1957) 549];
  Z. Maki, M. Nakagawa and S. Sakata, Prog. Theor. Phys. 28 (1962) 870; B. Pontecorvo,
  Sov. Phys. JETP 26 (1968) 984 [Zh. Eksp. Teor. Fiz. 53 (1967) 1717]; V. N. Gribov and B. Pontecorvo, Phys. Lett. B 28 (1969) 493.
- [5] M. Apollonio et al. [CHOOZ Collaboration], Phys. Lett. B 466 (1999) 415
   [arXiv:hep-ex/9907037]; Eur. Phys. J. C 27 (2003) 331 [arXiv:hep-ex/0301017].
- [6] A. Bandyopadhyay, S. Choubey, S. Goswami, S. T. Petcov and D. P. Roy, Phys. Lett. B 608 (2005) 115 [arXiv:hep-ph/0406328]; S. Goswami, A. Bandyopadhyay and S. Choubey, Nucl. Phys. Proc. Suppl. 143 (2005) 121 [arXiv:hep-ph/0409224].
- [7] M. C. Gonzalez-Garcia, arXiv:hep-ph/0410030.
- [8] A. Cervera, A. Donini, M. B. Gavela, J. J. Gomez Cadenas, P. Hernandez, O. Mena and S. Rigolin, Nucl. Phys. B 579 (2000) 17 [Erratum-ibid. B 593 (2001) 731] [arXiv:hep-ph/0002108].
- J. Burguet-Castell, M. B. Gavela, J. J. Gomez-Cadenas, P. Hernandez and O. Mena,
   Nucl. Phys. B 608 (2001) 301 [arXiv:hep-ph/0103258]; Nucl. Phys. B 646, 301 (2002)
   [arXiv:hep-ph/0207080].
- [10] H. Minakata and H. Nunokawa, JHEP **0110** (2001) 001 [arXiv:hep-ph/0108085].
- [11] G. L. Fogli and E. Lisi, Phys. Rev. D 54 (1996) 3667 [arXiv:hep-ph/9604415].
- [12] V. Barger, D. Marfatia and K. Whisnant, Phys. Rev. D **65** (2002) 073023 [arXiv:hep-ph/0112119].
- [13] Y. Itow et al., arXiv:hep-ex/0106019.
- [14] P. Zucchelli, Phys. Lett. B **532** (2002) 166.
- [15] S. Geer, Phys. Rev. D 57 (1998) 6989 [Erratum-ibid. D 59 (1999) 039903]
   [arXiv:hep-ph/9712290]; A. De Rujula, M. B. Gavela and P. Hernandez, Nucl. Phys. B 547 (1999) 21 [arXiv:hep-ph/9811390].
- [16] M. Apollonio *et al.*, arXiv:hep-ph/0210192.
- [17] P. Huber, M. Maltoni and T. Schwetz, Phys. Rev. D **71** (2005) 053006 [arXiv:hep-ph/0501037]; A. de Gouvea, J. Jenkins and B. Kayser, arXiv:hep-ph/0503079; H. Nunokawa, S. Parke and R. Z. Funchal, arXiv:hep-ph/0503283; O. Mena and S. Parke, arXiv:hep-ph/0505202.
- [18] P. Huber, M. Lindner and W. Winter, Nucl. Phys. B **645** (2002) 3 [arXiv:hep-ph/0204352].

- [19] J. Burguet-Castell, D. Casper, E. Couce, J. J. Gomez-Cadenas and P. Hernandez, arXiv:hep-ph/0503021.
- [20] J. J. Gomez-Cadenas *et al.* [CERN working group on Super Beams Collaboration], arXiv:hep-ph/0105297.
- [21] J. Bouchez, M. Lindroos and M. Mezzetto, AIP Conf. Proc. 721 (2004) 37 [arXiv:hep-ex/0310059]; M. Mezzetto, Nucl. Phys. Proc. Suppl. 143 (2005) 309 [arXiv:hep-ex/0410083].
- [22] C. K. Jung, arXiv:hep-ex/0005046.
- [23] A. Donini, D. Meloni and P. Migliozzi, Nucl. Phys. B 646 (2002) 321 [arXiv:hep-ph/0206034]; J. Phys. G 29 (2003) 1865 [arXiv:hep-ph/0209240].
- [24] A. Cervera, F. Dydak and J. Gomez Cadenas, Nucl. Instrum. Meth. A 451 (2000) 123.
- [25] D. Autiero et al., Eur. Phys. J. C 33 (2004) 243 [arXiv:hep-ph/0305185]; A. Donini, AIP Conf. Proc. 721 (2004) 219 [arXiv:hep-ph/0310014].
- [26] J. Burguet-Castell, D. Casper, J. J. Gomez-Cadenas, P. Hernandez and F. Sanchez, Nucl. Phys. B 695, 217 (2004) [arXiv:hep-ph/0312068].
- [27] A. Donini, E. Fernández-Martínez, P. Migliozzi, S. Rigolin and L. Scotto Lavina, Nucl. Phys. B **710** (2005) 402 [arXiv:hep-ph/0406132]; S. Rigolin, arXiv:hep-ph/0407009.
- [28] D. Casper, Nucl. Phys. Proc. Suppl. 112 (2002) 161 [arXiv:hep-ph/0208030].
- [29] J. Serreau and C. Volpe, Phys. Rev. C 70, 055502 (2004) [arXiv:hep-ph/0403293].
- [30] F. Terranova, A. Marotta, P. Migliozzi and M. Spinetti, Eur. Phys. J. C 38, 69 (2004) [arXiv:hep-ph/0405081].
- [31] T. Nakaya, Nucl. Phys. Proc. Suppl. **143** (2005) 96.
- [32] S. E. Kopp, arXiv:hep-ex/0412052.
- [33] K. Kodama [OPERA Collaboration], AIP Conf. Proc. 721 (2004) 231.
- [34] S. Gilardoni, CERN Thesis; S. Gilardoni, G. Grawer, G. Maire, J. M. Maugain, S. Rangod and F. Voelker, J. Phys. G 29 (2003) 1801.
- [35] J. E. Campagne and A. Cazes, arXiv:hep-ex/0411062.
- [36] A. Blondel et al., Nucl. Instrum. Meth. A 451 (2000) 102.
- [37] G. P. Zeller, arXiv:hep-ex/0312061.
- [38] P. Lipari, private communication; P. Lipari, M. Lusignoli and F. Sartogo, Phys. Rev. Lett. **74**, 4384 (1995) [arXiv:hep-ph/9411341].
- [39] M. C. Gonzalez-Garcia and C. Peña-Garay, Phys. Rev. D 68, 093003 (2003) [arXiv:hep-ph/0306001]; J. N. Bahcall, M. C. Gonzalez-Garcia and C. Peña-Garay, JHEP 0408, 016 (2004) [arXiv:hep-ph/0406294].

- [40] G. L. Fogli, E. Lisi and A. Palazzo, Phys. Rev. D **65** (2002) 073019 [arXiv:hep-ph/0105080].
- [41] S. Choubey, arXiv:hep-ph/0402288.
- [42] A. Donini, E. Fernández-Martínez and S. Rigolin, in preparation.
- [43] V. D. Barger, S. Geer and K. Whisnant, Phys. Rev. D 61 (2000) 053004 [arXiv:hep-ph/9906487]; V. D. Barger, S. Geer, R. Raja and K. Whisnant, Phys. Rev. D 62 (2000) 013004 [arXiv:hep-ph/9911524].
- [44] A. Bueno, M. Campanelli and A. Rubbia, Nucl. Phys. B **589** (2000) 577 [arXiv:hep-ph/0005007].
- [45] A. M. Dziewonski and D. L. Anderson, Phys. Earth Planet. Interiors 25 (1981) 297.
- [46] D. Meloni, Acta Phys. Polon. B 35, 2781 (2004).
- [47] A. Donini, D. Meloni and S. Rigolin, JHEP **0406**, 011 (2004) [arXiv:hep-ph/0312072].
- [48] A. Donini, E. Fernández-Martínez and S. Rigolin, arXiv:hep-ph/0411402; S. Rigolin, arXiv:hep-ph/0411403.
- [49] F. Ardellier *et al.*, arXiv:hep-ex/0405032.
- [50] H. Minakata, M. Sonoyama and H. Sugiyama, Phys. Rev. D 70, 113012 (2004) [arXiv:hep-ph/0406073].
- [51] E. K. Akhmedov et al., JHEP **0404** (2004) 078 [arXiv:hep-ph/0402175].
- [52] G. J. Feldman and R. D. Cousins, Phys. Rev. D 57 (1998) 3873 [arXiv:physics/9711021].
- [53] P. Huber, M. Lindner and W. Winter, arXiv:hep-ph/0412199.

## Appendix B: three-parameters fits

In this Appendix we present the projection of the three-dimensional 90% CL contours onto the  $(\theta_{13}, \delta)$  plane for the three reference setups (the low- $\gamma$   $\beta$ -Beam, the SPL Super-Beam and the 50 GeV Neutrino Factory) for different choices of the input pair  $(\bar{\theta}_{13}, \bar{\delta})$ . The external input parameters in all plots are:  $\theta_{12} = 32^{\circ}$ ,  $\Delta m_{12}^2 = 8.2 \times 10^{-5} \text{ eV}^2$ ;  $\theta_{23} = 40^{\circ}$ ,  $\Delta m_{23}^2 = 2.5 \times 10^{-3} \text{ eV}^2$ . In this case, all choices of the two discrete variables  $s_{atm}$  and  $s_{oct}$  are presented together and no comparison with two-parameters contours is shown.

For the  $\beta$ -Beam plots we compare the impact of the present uncertainties on the atmospheric parameters (third column of Tab. 1) with that of the expected uncertainties after T2K-I (last column of Tab. 1):  $\theta_{23} \in [38^{\circ}, 43^{\circ}] - [48^{\circ}, 52^{\circ}]$  and  $\Delta m_{23}^2 \in [2.42, 2.61] \times 10^{-3} \text{ eV}^2$  for  $s_{atm} = +$  and  $\Delta m_{23}^2 \in [2.46, 2.64] \times 10^{-3} \text{ eV}^2$  for  $s_{atm} = -$ , [42]. Notice that the error on  $\theta_{23}$  is just the expected error at T2K-I, [13], shifted around  $\theta_{23} = 40^{\circ}$ . It has been shown in Sect. 5.2 that the  $\nu_{\mu}$  disappearance channel at the Super-Beam is rather effective in reducing the uncertainties on the atmospheric parameters (whereas the  $\nu_e$  disappearance channel at the low- $\gamma$   $\beta$ -Beam is useless to this purpose, see Ref. [48]). In this case we therefore do not present results using "present" and "expected" uncertainties, but we just combine the results from the appearance and disappearance channel. Finally, for the Neutrino Factory we have considered only the two appearance channels  $\nu_e \to \nu_{\mu}, \nu_{\tau}$  with the atmospheric parameters with the expected uncertainties after T2K-I.

In general, a "pessimistic" systematic error,  $\epsilon^{\pm} = 5\%$ , has been used in appearance channels. A 2% systematic error has been used in disappearance channels. However, we checked that using a "pessimistic" 5% systematic error in the disappearance channel does not change significantly our results.

The input parameters are:  $\bar{\theta}_{13} = 2^{\circ}, 7^{\circ}; \bar{\delta} = 90^{\circ}, 45^{\circ}, 0^{\circ}, -45^{\circ}, -90^{\circ}.$ 

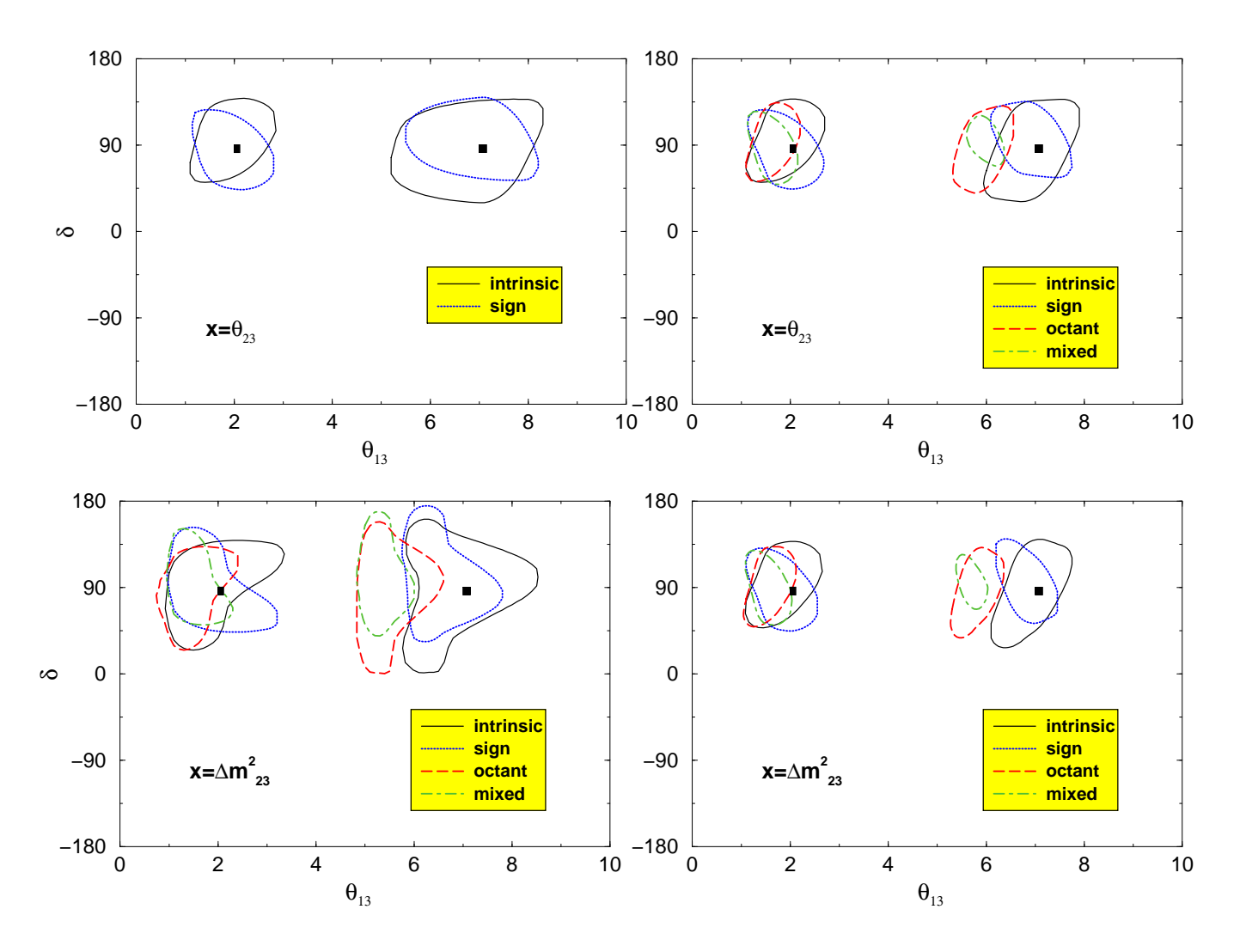


Fig. 12. Three-parameters 90 % CL contours after a 10 years run at the  $\beta$ -Beam. Input parameters:  $\bar{\theta}_{13} = 2^{\circ}, 7^{\circ}$ ;  $\bar{\delta} = 90^{\circ}$ . Top panels:  $x = \theta_{23}$ ; bottom panels:  $x = \Delta m_{23}^2$ . Left panels: present uncertaintes; right panels: after T2K-I.

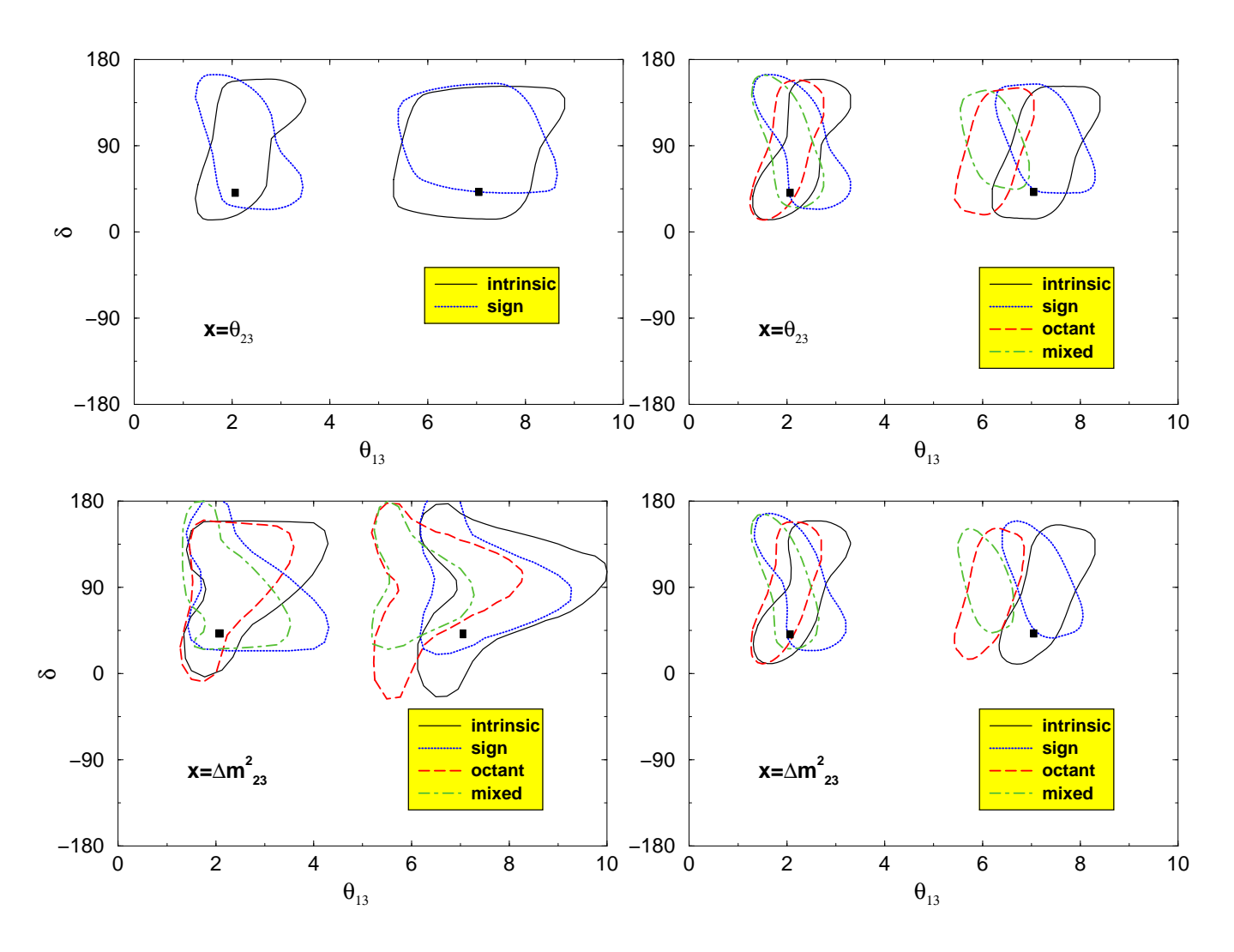


Fig. 13. Three-parameters 90 % CL contours after a 10 years run at the  $\beta$ -Beam. Input parameters:  $\bar{\theta}_{13} = 2^{\circ}, 7^{\circ}$ ;  $\bar{\delta} = 45^{\circ}$ . Top panels:  $x = \theta_{23}$ ; bottom panels:  $x = \Delta m_{23}^2$ . Left panels: present uncertaintes; right panels: after T2K-I.

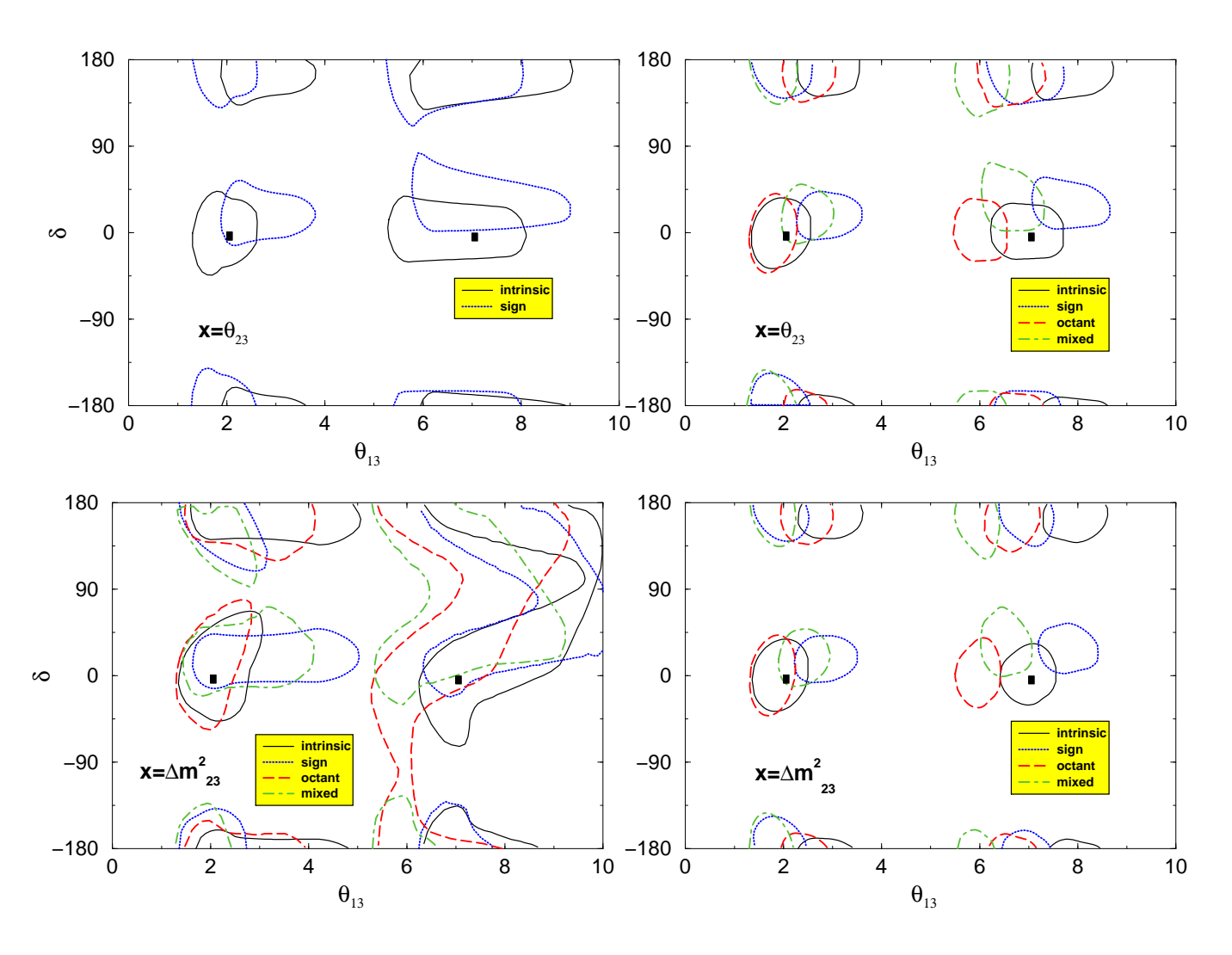


Fig. 14. Three-parameters 90 % CL contours after a 10 years run at the  $\beta$ -Beam. Input parameters:  $\bar{\theta}_{13} = 2^{\circ}, 7^{\circ}$ ;  $\bar{\delta} = 0^{\circ}$ . Top panels:  $x = \theta_{23}$ ; bottom panels:  $x = \Delta m_{23}^2$ . Left panels: present uncertaintes; right panels: after T2K- I.

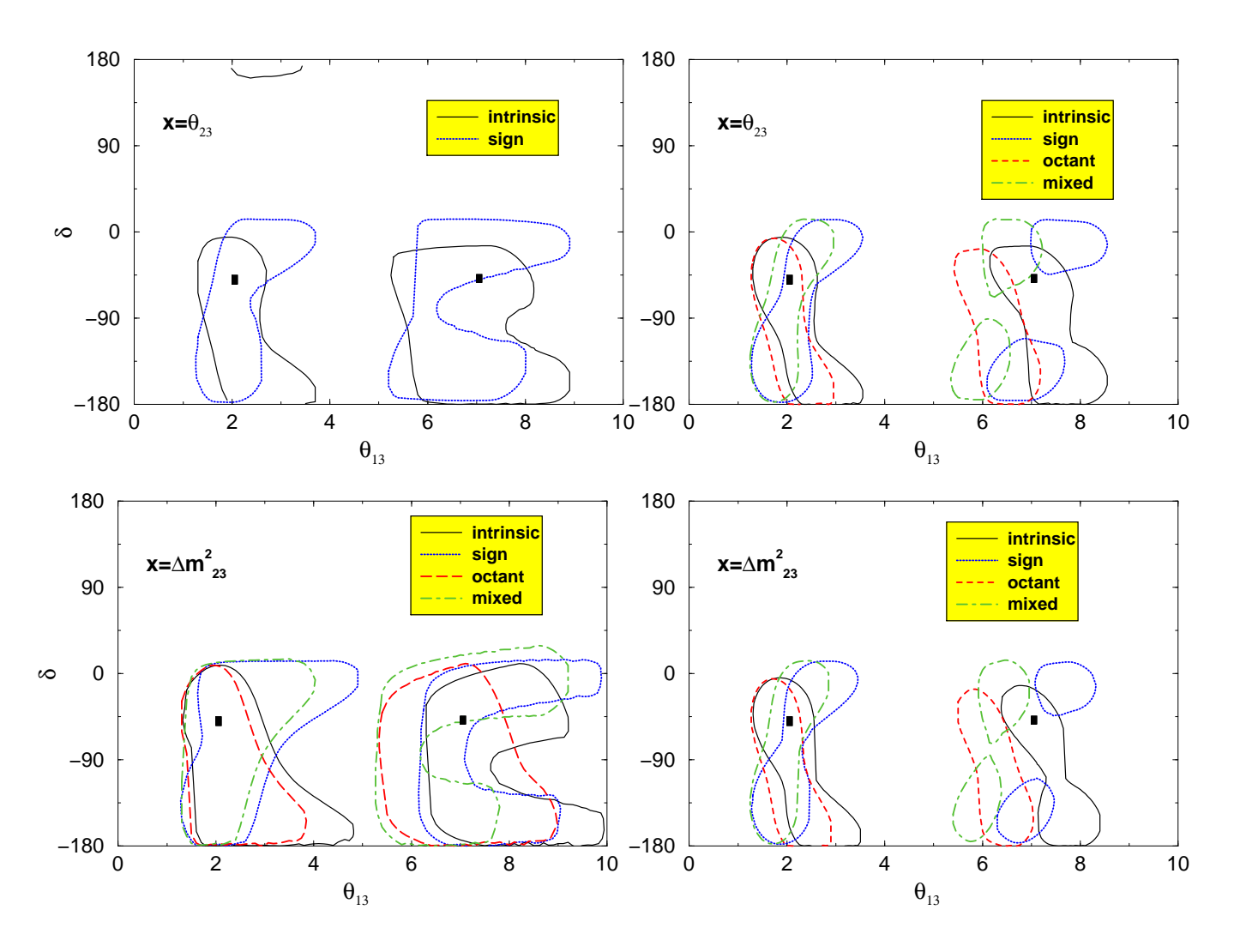


Fig. 15. Three-parameters 90 % CL contours after a 10 years run at the  $\beta$ -Beam. Input parameters:  $\bar{\theta}_{13} = 2^{\circ}, 7^{\circ}$ ;  $\bar{\delta} = -45^{\circ}$ . Top panels:  $x = \theta_{23}$ ; bottom panels:  $x = \Delta m_{23}^2$ . Left panels: present uncertaintes; right panels: after T2K-I.

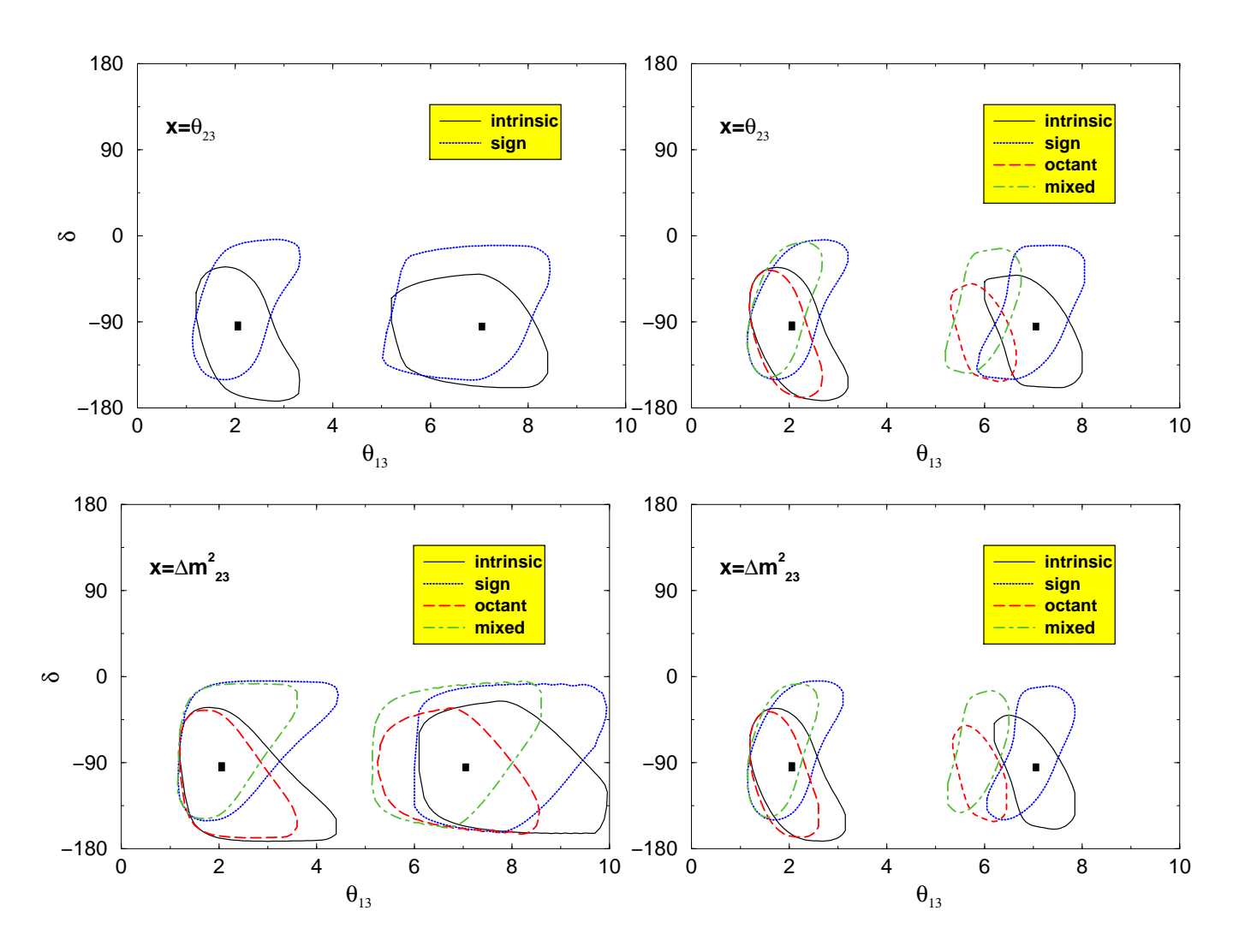


Fig. 16. Three-parameters 90 % CL contours after a 10 years run at the  $\beta$ -Beam. Input parameters:  $\bar{\theta}_{13} = 2^{\circ}, 7^{\circ}$ ;  $\bar{\delta} = -90^{\circ}$ . Top panels:  $x = \theta_{23}$ ; bottom panels:  $x = \Delta m_{23}^2$ . Left panels: present uncertaintes; right panels: after T2K-I.

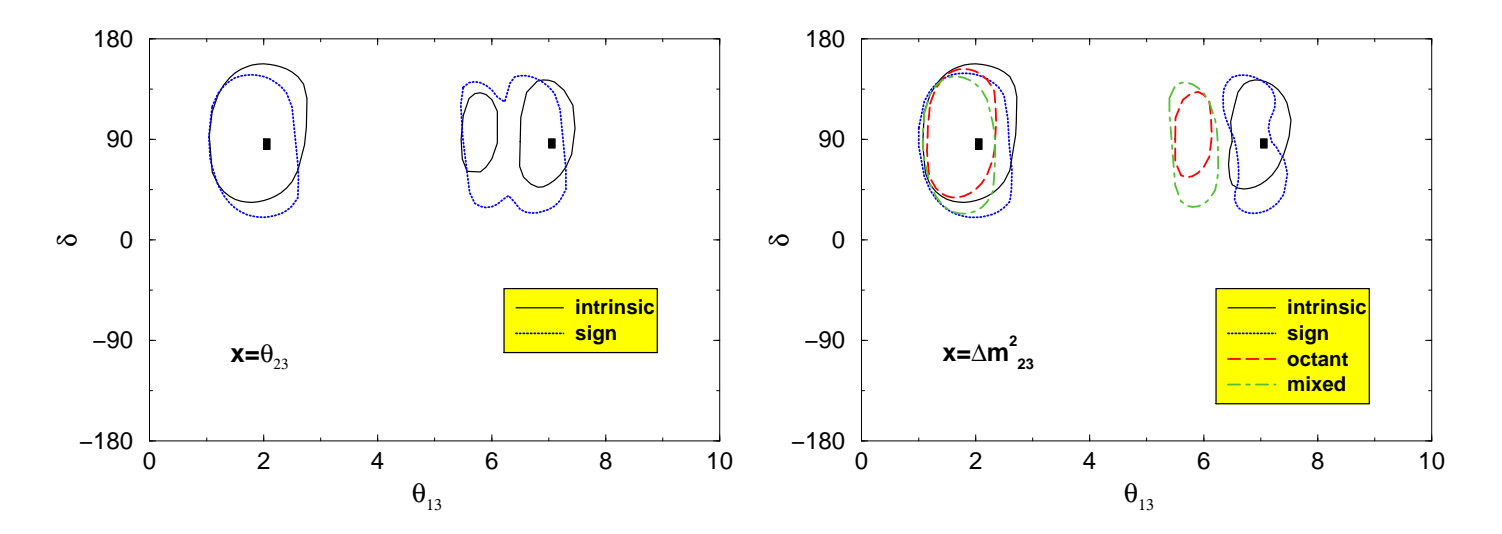


Fig. 17. Three-parameters 90 % CL contours after a 2+8 years run at the Super-Beam. Input parameters:  $\bar{\theta}_{13}=2^{\circ},7^{\circ}; \bar{\delta}=90^{\circ}$ . Left:  $x=\theta_{23};$  right:  $x=\Delta m_{23}^2$ .

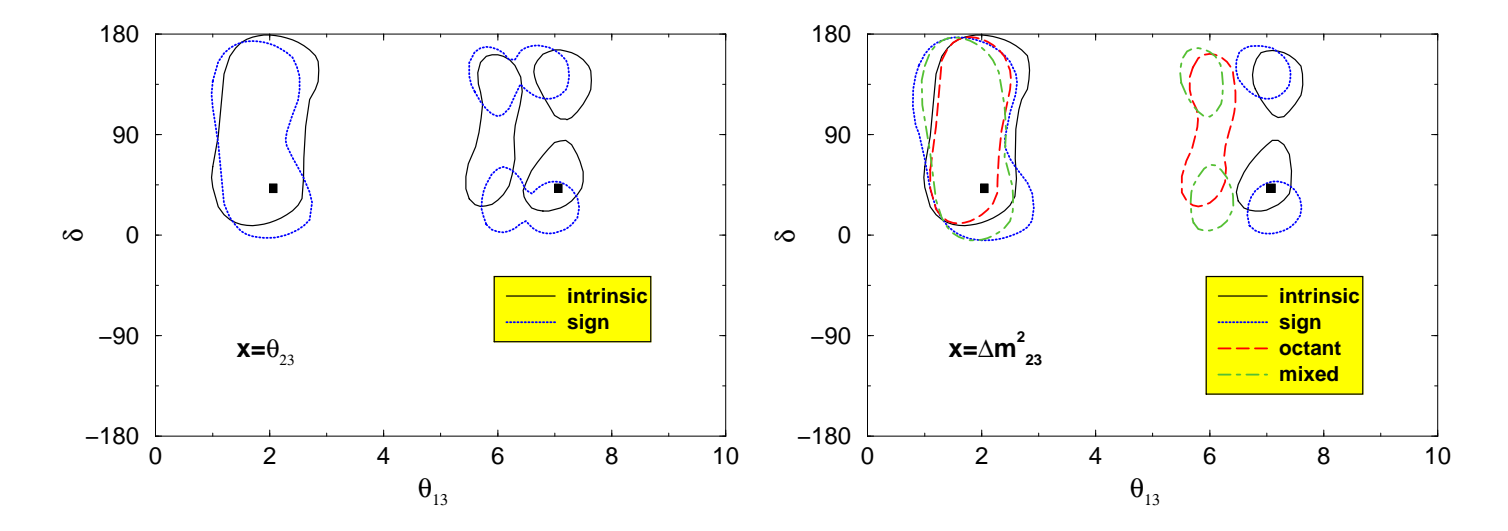


Fig. 18. Three-parameters 90 % CL contours after a 2+8 years run at the Super-Beam. Input parameters:  $\bar{\theta}_{13} = 2^{\circ}, 7^{\circ}; \bar{\delta} = 45^{\circ}$ . Left:  $x = \theta_{23};$  right:  $x = \Delta m_{23}^2$ .

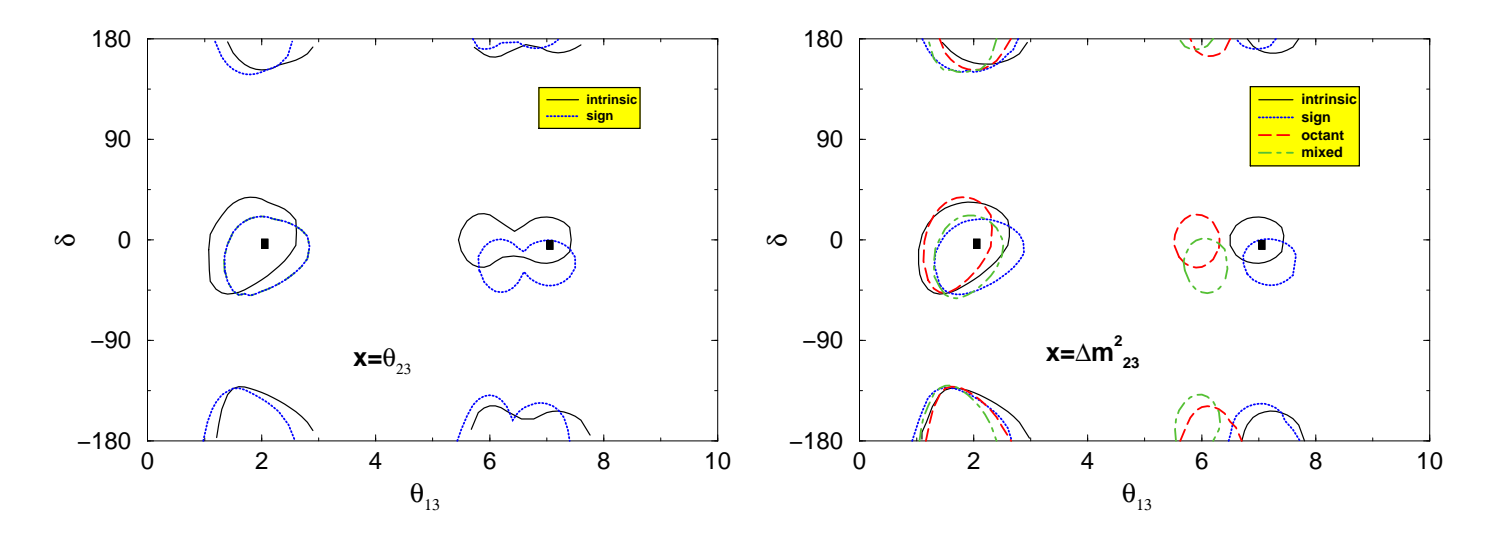


Fig. 19. Three-parameters 90 % CL contours after a 2+8 years run at the Super-Beam. Input parameters:  $\bar{\theta}_{13} = 2^{\circ}, 7^{\circ}; \bar{\delta} = 0^{\circ}$ . Left:  $x = \theta_{23}$ ; right:  $x = \Delta m_{23}^2$ .

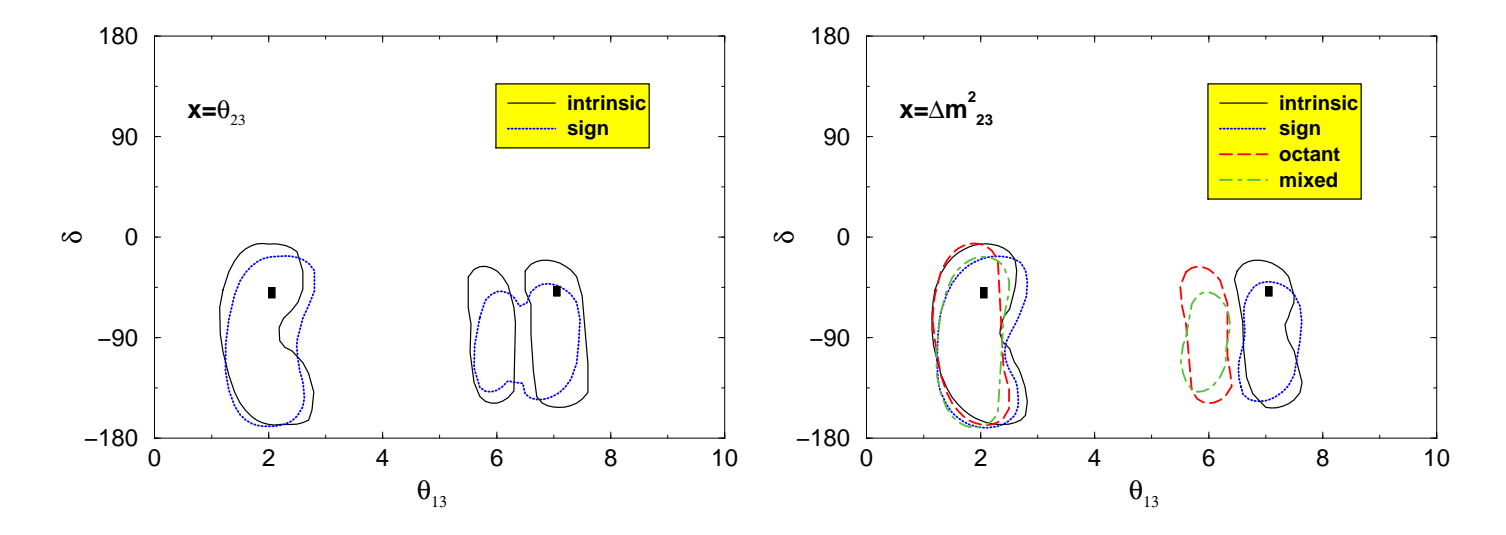


Fig. 20. Three-parameters 90 % CL contours after a 2+8 years run at the Super-Beam. Input parameters:  $\bar{\theta}_{13} = 2^{\circ}, 7^{\circ}; \bar{\delta} = -45^{\circ}$ . Left:  $x = \theta_{23};$  right:  $x = \Delta m_{23}^2$ .

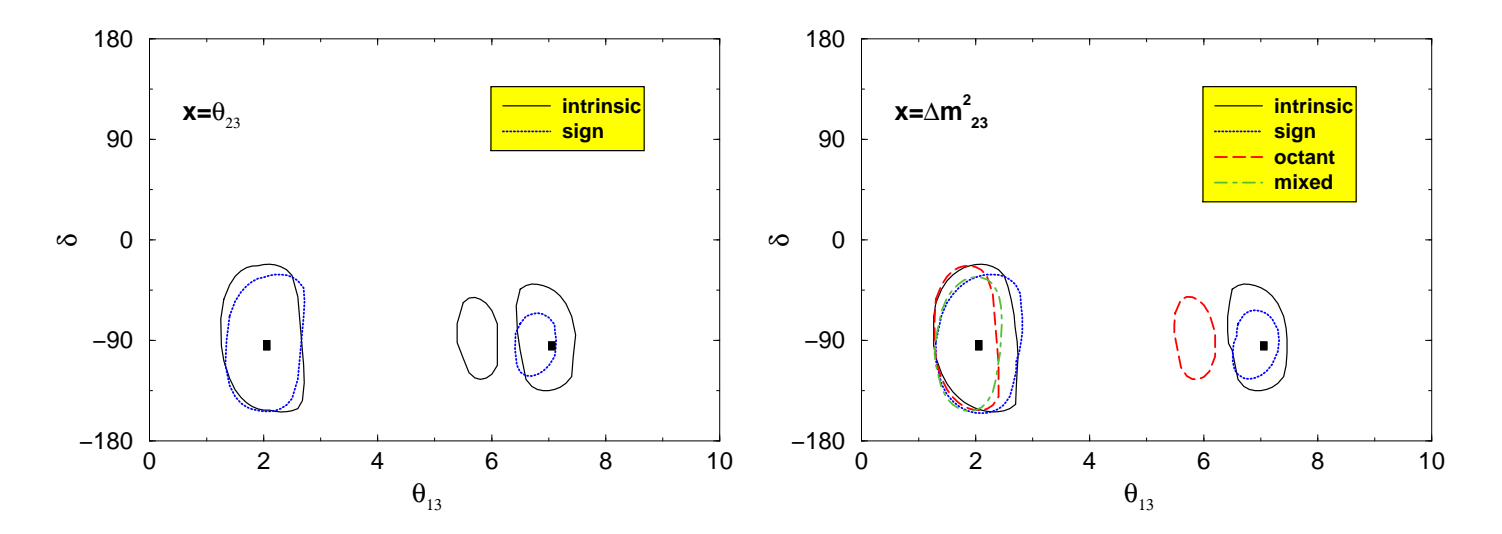


Fig. 21. Three-parameters 90 % CL contours after a 2+8 years run at the Super-Beam. Input parameters:  $\bar{\theta}_{13} = 2^{\circ}, 7^{\circ}; \bar{\delta} = -90^{\circ}$ . Left:  $x = \theta_{23}; right: x = \Delta m_{23}^2$ .

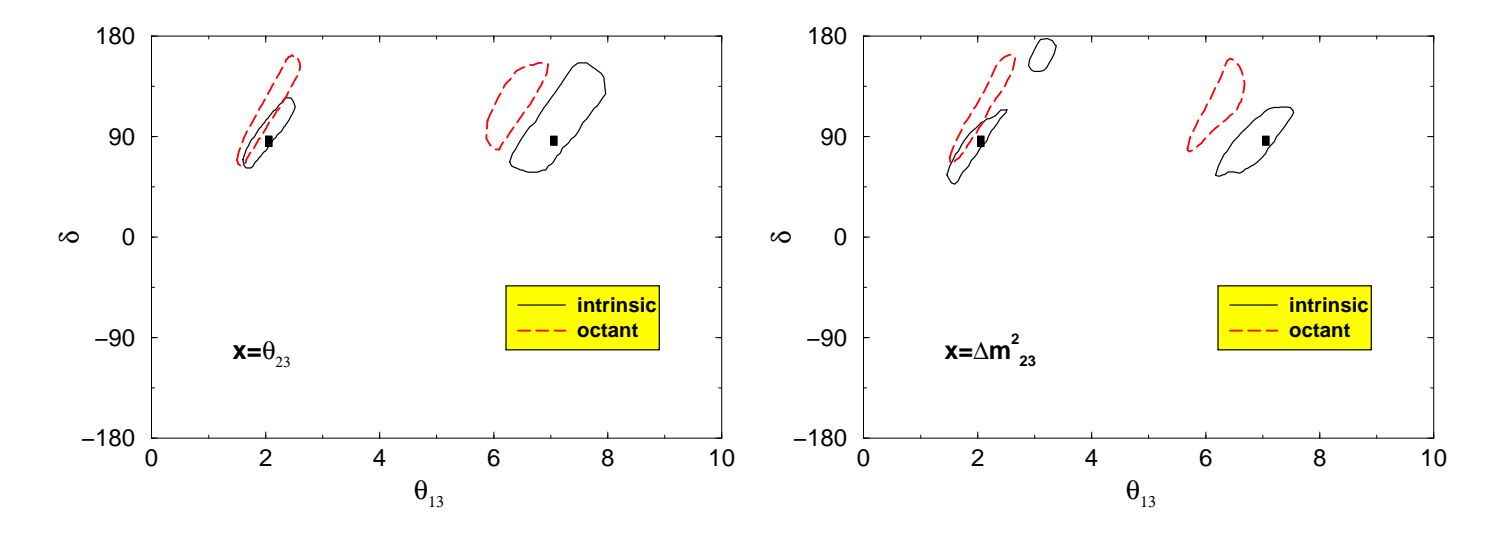


Fig. 22. Three-parameters 90 % CL contours after a 5+5 years run at the Neutrino Factory. Input parameters:  $\bar{\theta}_{13}=2^{\circ},7^{\circ}; \ \bar{\delta}=90^{\circ}$ . Left:  $x=\theta_{23}; \ right: x=\Delta m_{23}^2$ .

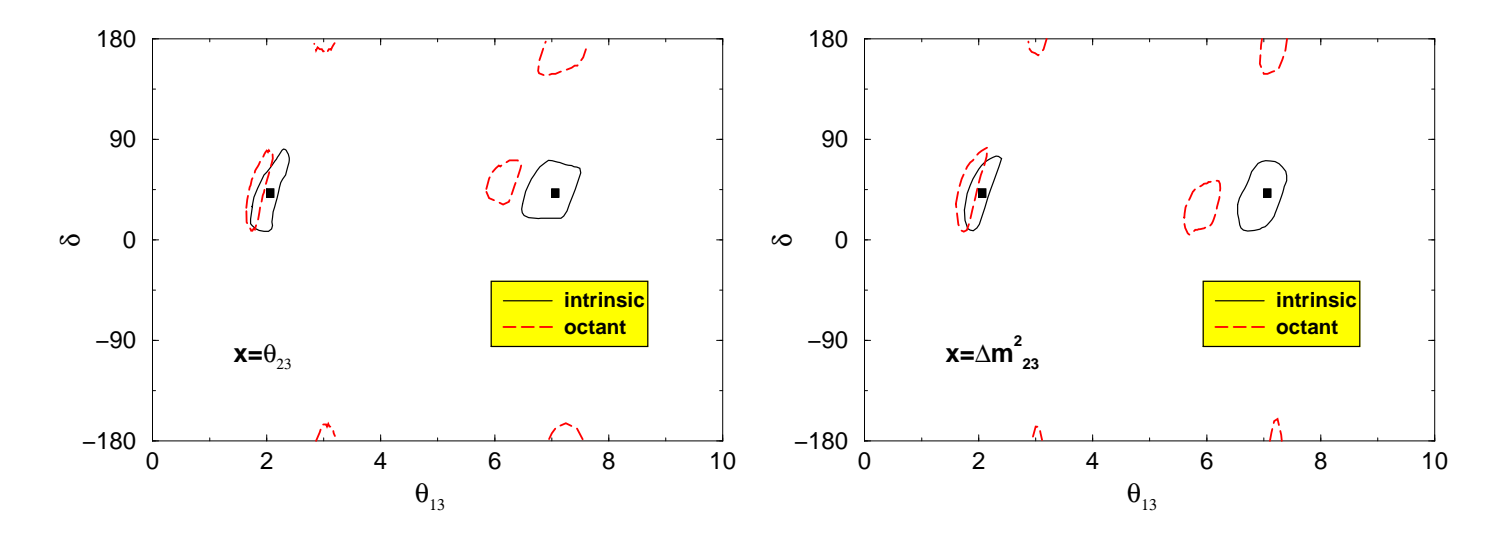


Fig. 23. Three-parameters 90 % CL contours after a 5+5 years run at the Neutrino Factory. Input parameters:  $\bar{\theta}_{13}=2^{\circ},7^{\circ};\ \bar{\delta}=45^{\circ}$ . Left:  $x=\theta_{23};$  right:  $x=\Delta m_{23}^2$ .

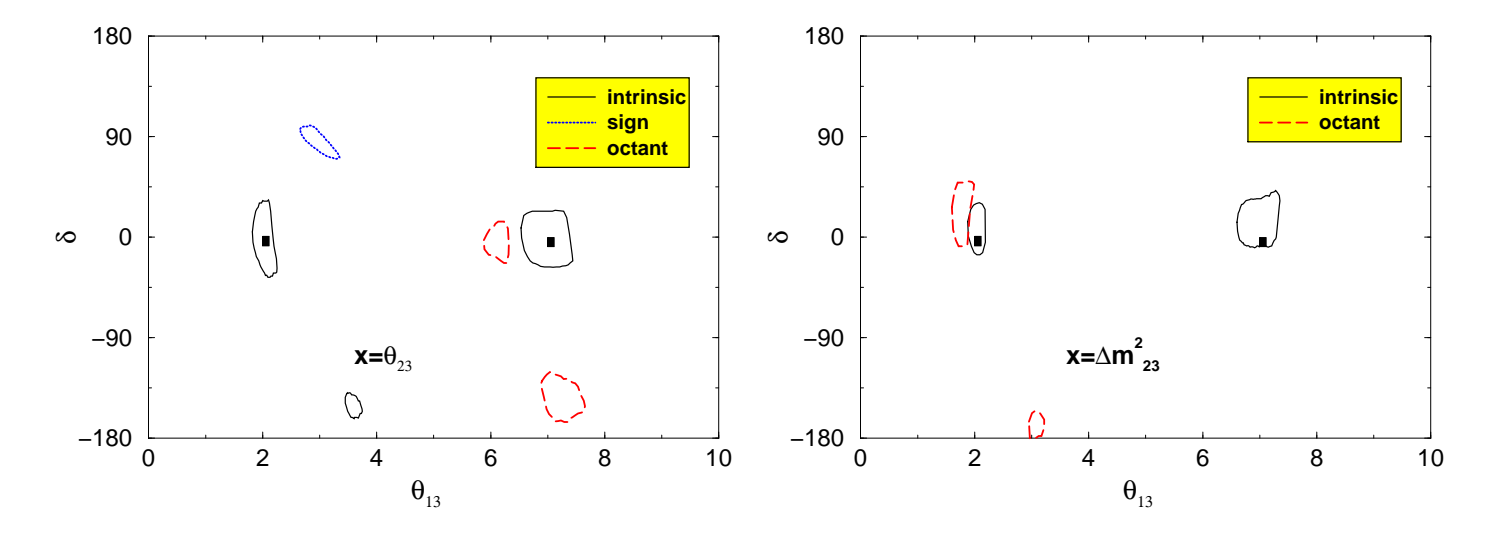


Fig. 24. Three-parameters 90 % CL contours after a 5+5 years run at the Neutrino Factory. Input parameters:  $\bar{\theta}_{13} = 2^{\circ}, 7^{\circ}; \bar{\delta} = 0^{\circ}$ . Left:  $x = \theta_{23}$ ; right:  $x = \Delta m_{23}^2$ .

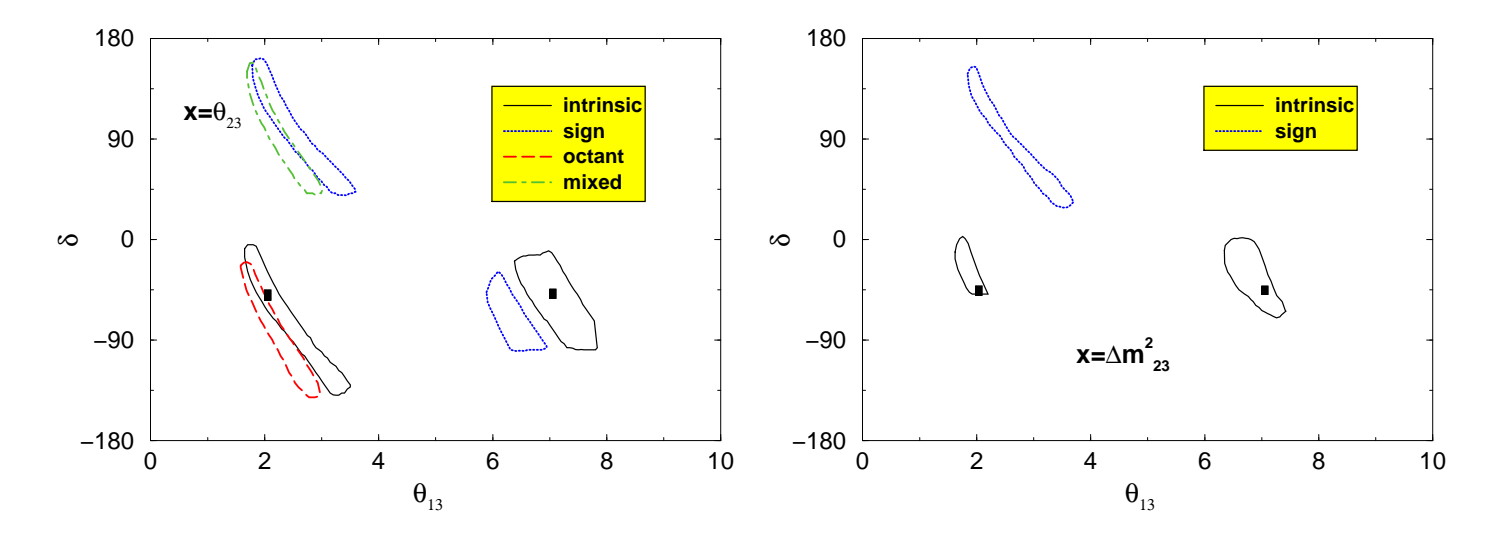


Fig. 25. Three-parameters 90 % CL contours after a 5+5 years run at the Neutrino Factory. Input parameters:  $\bar{\theta}_{13}=2^{\circ},7^{\circ};\ \bar{\delta}=-45^{\circ}$ . Left:  $x=\theta_{23};\ right:\ x=\Delta m_{23}^2$ .

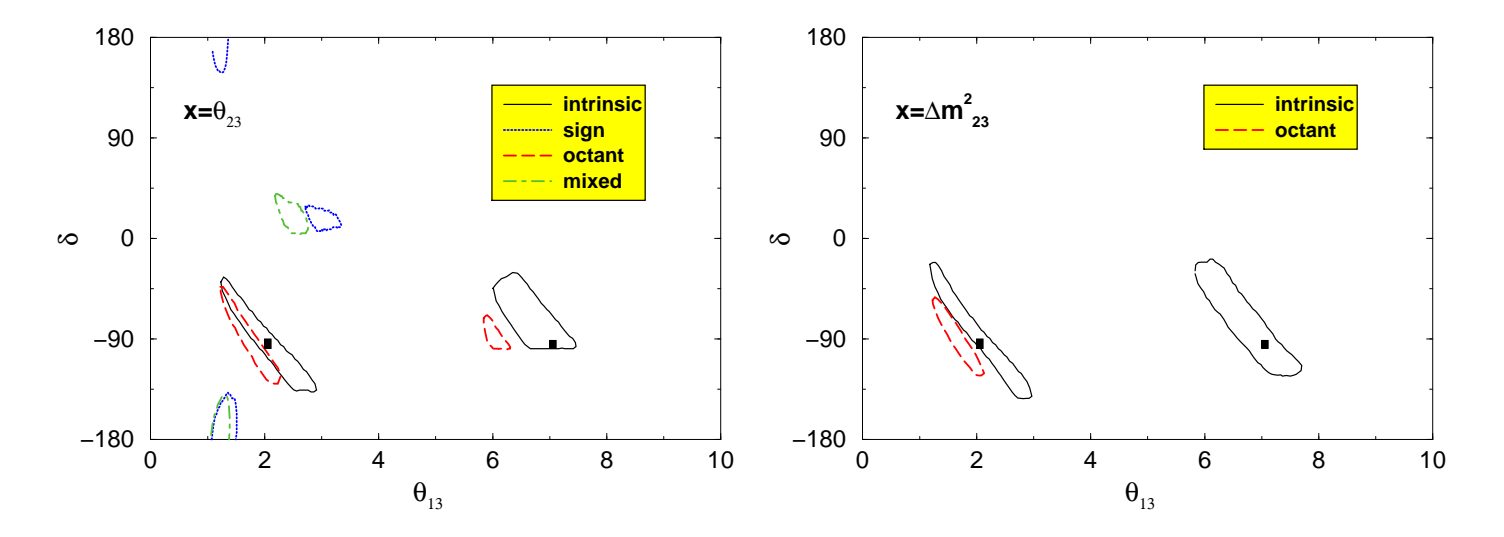


Fig. 26. Three-parameters 90 % CL contours after a 5+5 years run at the Neutrino Factory. Input parameters:  $\bar{\theta}_{13} = 2^{\circ}, 7^{\circ}; \ \bar{\delta} = -90^{\circ}$ . Left:  $x = \theta_{23}; \ right: x = \Delta m_{23}^2$ .